

Response of Marine-Terminating Glaciers to Forcing: Time Scales, Sensitivities, Instabilities and Stochastic Dynamics

Alexander A. Robel^{1,2}, Gerard H. Roe³, Marianne Haseloff^{4,5}

¹School of Earth and Atmospheric Sciences, Georgia Institute of Technology

²Division of Geological and Planetary Sciences, California Institute of Technology

³Department of Earth and Space Sciences, University of Washington

⁴AOS Program, Princeton University

⁵Department of Earth Sciences, University of Oxford

Key Points:

- The marine-terminating glacier response to forcing occurs on two distinct time scales
- The glacier sensitivity to forcing depends on glacier state and nonlinearity in forcing processes
- The level of noise in nonlinear forcing processes can change the equilibrium state of a glacier

Corresponding author: Alexander A. Robel, 311 Ferst Drive, Atlanta, GA, USA, 30318,
robela@eas.gatech.edu

Abstract

Recent observations indicate that many marine-terminating glaciers in Greenland and Antarctica are currently retreating and thinning, potentially due to long-term trends in climate forcing. In this study, we describe a simple two-stage model that accurately emulates the response to external forcing of marine-terminating glaciers simulated in a spatially-extended model. The simplicity of the model permits derivation of analytical expressions describing the marine-terminating glacier response to forcing. We find that there are two time scales that characterize the stable glacier response to external forcing, a fast time scale of decades to centuries, and a slow time scale of millennia. These two time scales become unstable at different thresholds of bed slope, indicating that there are distinct slow and fast forms of the marine ice sheet instability. We derive simple expressions for the approximate magnitude and transient evolution of the stable glacier response to external forcing, which depend on the equilibrium glacier state and the strength of nonlinearity in forcing processes. The slow response rate of marine-terminating glaciers indicates that current changes at some glaciers are set to continue and accelerate in coming centuries in response to past climate forcing, and that the current extent of change at these glaciers is likely a small fraction of the future committed change caused by past climate forcing. Finally, we find that changing the amplitude of natural fluctuations in some nonlinear forcing processes, such as ice-shelf calving, changes the equilibrium glacier state.

1 Introduction

Marine-terminating glaciers transport ice from the interior of ice sheets towards the ocean where ice melts or fractures into icebergs. Recent observations indicate that changes are underway in the speed, thickness and terminus position of many marine-terminating glaciers in Greenland [Bjørk *et al.*, 2012; Moon *et al.*, 2015; Felikson *et al.*, 2017] and Antarctica [Pritchard *et al.*, 2009; Scheuchl *et al.*, 2016]. These changes are thought to be caused by long-term trends in climate which drive surface melting [Fettweis, 2007; Velicogna, 2009; Mernild *et al.*, 2011], ocean melting [Rignot *et al.*, 2010; Joughin *et al.*, 2012] and accelerated iceberg calving [Joughin *et al.*, 2008; Nick *et al.*, 2010].

It has long been understood that glaciers act as integrators of external forcing [Nye, 1960, 1963a,b, 1965]. Stochastic noise in climate forcing is integrated by glaciers on a characteristic time scale set by glacier mass balance and geometry [Jóhannesson *et al.*, 1989; Harrison *et al.*, 2003], causing fluctuations of glacier thickness, flux and length that

48 are superimposed on the background glacier state [*Oerlemans, 2000; Lüthi, 2009; Roe*
49 *and Baker, 2014*]. Glaciers also respond to persistent changes in climate forcing on this
50 characteristic time scale. Consequently, to evaluate whether recent retreat at individual
51 mountain glaciers is caused by climate change or interannual variability, studies have com-
52 pared the amplitude of stationary glacier variability (i.e. variability drawn from a distri-
53 bution whose properties do not change in time) to the magnitude of non-stationary glacier
54 changes caused by persistent trends in climate [*Oerlemans, 2000; Roe and O’Neal, 2009;*
55 *Marzeion et al., 2014; Roe et al., 2017*]. However, such comparisons are inherently diffi-
56 cult where records of glacier change are short compared to the slow response of glaciers
57 to climate change.

58 In practice, complex numerical ice-sheet models are used to calculate the discharge
59 of ice from glaciers and predict the long-term response of marine-terminating glaciers to
60 future climate change [e.g., *Pattyn et al., 2012; Favier et al., 2014; Seroussi et al., 2017*].
61 However, recent studies have provided simple analytical expressions for the dependence of
62 ice discharge on local topographic and glaciological conditions, derived from asymptotic
63 analysis of glacier flow at the grounding line [*Schoof, 2007a; Hindmarsh, 2012; Tsai et al.,*
64 *2015; Pegler, 2016; Schoof et al., 2017; Haseloff and Sergienko, 2018*]. The balance be-
65 tween ice input from snowfall and ice discharge to the ocean sets the equilibrium glacier
66 state and determines the stability of marine ice-sheet grounding lines [*Schoof, 2012*].
67 Consequently, these simple approximations for ice discharge are potentially useful tools
68 for simulating marine-terminating glacier change without using a complex ice-sheet model.

69 Simulations of non-stationary change in marine-terminating glaciers often neglect
70 the stationary, high-frequency variability in climate forcing. However, *Mantelli et al.* [2016]
71 showed that in marine-terminating glaciers with internally-generated variability, the inclu-
72 sion of realistic noise in accumulation and surface temperature forcing may cause vari-
73 ability at decadal to centennial time scales that do not arise in the absence of noise. *Mul-*
74 *der et al.* [2018] showed that noisy forcing can cause grounding lines to transition across
75 reverse-sloping beds, with the likelihood of unstable retreat found to be greater than the
76 likelihood of unstable advance. Such studies raise the possibility that together, noisy forc-
77 ing and the internal dynamics of glacier flow, produce glacier variability that should be
78 considered when interpreting and simulating glacier change due to climate forcing.

79 In this study, we show that a simple model of ice fluxes in a marine-terminating
 80 glacier can accurately emulate the most significant components of stochastic and non-
 81 stationary variability that appear in a flowline model (Section 2). We show (Section 3)
 82 that stable marine-terminating glaciers respond to forcing on two characteristic time scales
 83 separated by one to two orders of magnitude. These time scales vary with equilibrium
 84 glacier state (which is set by internal dynamics) and become unstable at different thresh-
 85 olds of bed slope. We derive (Section 4) the glacier sensitivities to step, trend, and stochas-
 86 tic fluctuations in external forcing. These expressions for the glacier sensitivity provide a
 87 first-order approximation of the glacier response to forcing without the need for a com-
 88 plex numerical model. We show that these sensitivities depend on equilibrium glacier state
 89 and the strength of nonlinearity in forcing processes. Finally, we show (Section 5) that
 90 under certain circumstances, equilibrium glacier state depends on the strength of noisy
 91 forcing, indicating that marine-terminating glaciers are nonlinear, state-dependent integra-
 92 tors of external forcing. We conclude (Section 6) with a discussion of the relevance of
 93 the time-scales and sensitivities of the two-stage model, to observed variability of marine-
 94 terminating glaciers in Greenland and Antarctica. We also suggest approaches for simu-
 95 lating future marine-terminating glacier behavior that consider the role of noise in climate
 96 forcing and ice-sheet processes.

97 **2 Two-stage marine-terminating glacier model**

98 High-order numerical models are typically used to simulate the response of marine-
 99 terminating glaciers to external forcing [e.g., *Pattyn et al.*, 2012; *Favier et al.*, 2014; *Seroussi*
 100 *et al.*, 2017]. In this section, we show that a simple, two-stage model of a marine-terminating
 101 glacier (i.e. two stages of adjustment) can accurately emulate the forced variability simu-
 102 lated in a more complex model. This two-stage model clearly shows the role of different
 103 physical processes in the glacier response to forcing, and is also simple enough to permit
 104 derivation of the characteristic time scales (Section 3) and sensitivities to different types
 105 of forcing (Section 4). We begin with the derivation of the two-stage model.

106 **2.1 Model derivation and assumptions**

107 The organizing principle of our two-stage model is tracking how ice enters, moves
 108 through, and then exits a marine-terminating glacier. We consider a marine-terminating
 109 glacier with length L and spatially-averaged thickness H (schematic in Figure 1b). The

length L spans the entire glacier domain from the ice divide (where there is no horizontal ice flow) to the grounding line. Consequently, we can take the total glacier ice volume to be $V = HLW$ where W is spatially-averaged glacier width. The only way ice enters the glacier is through accumulation due to spatially-averaged surface mass balance, P (the sum of accumulation and melting on the glacier surface). Ice leaves the glacier through a grounding line flux (Q_g),

$$\frac{dV}{dt} = W(P L - Q_g). \quad (1)$$

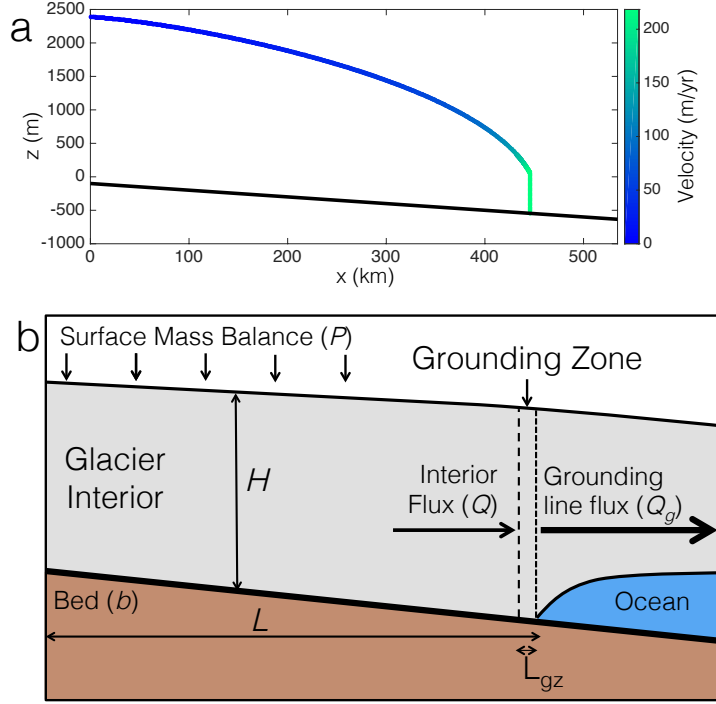
Carrying through the derivative, we re-arrange to arrive at an equation for the evolution of spatially-averaged glacier thickness

$$\frac{dH}{dt} = P - \frac{Q_g}{L} - \frac{H}{L} \frac{dL}{dt}. \quad (2)$$

where, physically, the terms on the right-hand side are: ice input due to spatially-averaged surface mass balance, ice output due to divergence of ice flux through the grounding line ($\frac{Q_g}{L}$), and stretching due to changes in overall glacier length ($\frac{H}{L} \frac{dL}{dt}$).

In this study, we only consider scenarios where the time- and spatially-averaged surface mass balance (\bar{P}) is greater than zero, leading to a finite glacier length at steady-state. We note however, that this does not exclude the possibility that the glacier can lose ice ($P < 0$) during transient time periods when surface melting exceeds accumulation through snowfall. We also note that climatological feedbacks may cause the surface mass balance to be dependent on variations in glacier geometry [as in *Harrison et al.*, 2003], though we do not include such effects here under the assumption that they are small compared to ice flux feedbacks. If the width of the glacier in the grounding zone is different from the average width of the upstream catchment area of the glacier, we could also include a geometric multiplier on the surface mass balance term (i.e. PW_{UP}/W_{GZ}), which accounts for the fact that wide catchment areas may be funneled into narrow glacier outlets near the grounding zone. We don't consider such geometric complications in the idealized analyses in this study, since the primary effect is to multiply the surface mass balance term. However, in using this simple model to approximate specific glaciers, such geometric considerations may be important.

The grounding zone is the region upstream of the grounding line (Figure 1b), with length L_{gz} , thickness h_g , and volume $V_{gz} = h_g L_{gz} W$. The grounding line is, by definition, the location where ice is sufficiently thin to float in seawater. Thus, the grounding-



138 **Figure 1.** (a) Example of a ice thickness and velocity profile simulated by a flowline model of a marine-
 139 terminating glacier. See section 2.2 for model description. (b) Schematic of two-stage model. The bed
 140 geometry shown in schematic is purely illustrative.

144 line ice thickness is exactly at hydrostatic equilibrium with the local water depth,

$$145 \quad h_g = -\lambda b(L), \quad (3)$$

146 where $\lambda = \rho_w/\rho_i$ is the ratio between the densities of seawater and glacial ice, and $b(L)$
 147 is the depth of the bed below sea level at the grounding line. Thus, our model implicitly
 148 assumes that the glacier always remains marine-terminating. In order to consider a glacier
 149 terminus that is not at flotation, we would need to substitute this condition with another
 150 dynamical equation for terminus ice thickness and calving rate [as in *Amundson, 2016*].
 151 The length of the grounding zone is typically a few kilometers (for flat ice streams it may
 152 be tens of kilometers), which is much shorter than the length of the entire glacier ($L_{gz} \ll$
 153 L). Considering a local conservation of ice mass in the grounding zone, we assume that
 154 ice is advected into the grounding zone from the interior (Q) and is discharged by flux
 155 through the grounding line (Q_g),

$$156 \quad \frac{dV_{gz}}{dt} = W(Q - Q_g), \quad (4)$$

157 where the additional flux from local surface mass balance (PL_{gz}) is assumed to be negli-
 158 gible. Carrying through the derivative on the left hand side, as we did for the large-scale
 159 glacier evolution equation (equation 2), we have

$$160 \quad h_g \frac{dL_{gz}}{dt} + L_{gz} \frac{dh_g}{dt} = Q - Q_g. \quad (5)$$

161 Since the grounding zone length is included within the full ice stream length ($L = L_{int} +$
 162 L_{gz} where L_{int} is a quantity that we assume changes negligibly compared to the ground-
 163 ing zone, where most longitudinal stretching occurs in marine-terminating glacier), stretch-
 164 ing and shrinking of the grounding zone length results in an equal change in glacier length
 165 (i.e. $dL/dt = dL_{gz}/dt$). We can then re-write equation 5 as

$$166 \quad (h_g - \lambda b_x L_{gz}) \frac{dL}{dt} = Q - Q_g, \quad (6)$$

167 where b_x is the local bed slope. Since b_x typically has the scale h_g/L [as assumed in
 168 *Schoof, 2007a*], we can generally say that $\lambda b_x L_{gz} \ll h_g$. Consequently, we can write the
 169 evolution equation for grounding line position as

$$170 \quad \frac{dL}{dt} = \frac{1}{h_g} (Q - Q_g). \quad (7)$$

171 Since the grounding zone is very short, the grounding line flux in equation 7 has the form
 172 of a moving flux boundary condition that sets the grounding-line position. Changes in
 173 grounding line position are directly caused by changes in the grounding zone flux balance
 174 ($Q - Q_g$), which may be influenced by far-field changes, such as fluctuations in upstream
 175 surface mass balance.

176 Equation 7 is combined with equation 2 to produce an evolution equation for the
 177 spatially-averaged glacier thickness (H)

$$178 \quad \frac{dH}{dt} = P - \frac{Q_g}{L} - \frac{H}{h_g L} (Q - Q_g). \quad (8)$$

179 Equations (7 and (8) form a complete two-stage dynamical model for the temporal evolu-
 180 tion of a marine-terminating glacier. In this two-stage marine-terminating glacier model,
 181 ice enters through a prescribed surface mass balance, flows through the ice-sheet interior
 182 towards the grounding zone and then leaves as a grounding-line flux. The first equation
 183 tracks the bulk mass flows through the marine-terminating glacier and the corresponding
 184 evolution of the glacier thickness. The second equation tracks the moving boundary con-
 185 dition at the downstream edge of the glacier that controls the magnitude of ice flux out of
 186 the glacier. The primary difference then, between this marine-terminating glacier model

187 and previous simple models of mountain glaciers [e.g., Jóhannesson *et al.*, 1989; Oerle-
 188 mans, 2000; Harrison *et al.*, 2003; Lüthi, 2009; Roe and Baker, 2014], is that mass loss
 189 occurs primarily through ice flux, rather than through negative surface mass balance. If
 190 these two equations have a stable solution, they must be associated with, at most, two dis-
 191 tinct time scales of glacier evolution (as we will see in section 3).

192 In marine-terminating outlet glaciers, ice in the glacier interior flows due to a com-
 193 bination of sliding at the base and deformation in the ice column. In this study, we will
 194 assume a very general form for interior ice flux

$$195 \quad Q = \nu \frac{H^\alpha}{L^\gamma}. \quad (9)$$

196 This form generally holds when ice flux is occurring through a balance between gravita-
 197 tional driving stress ($\rho_i g H \frac{\partial H}{\partial x}$) and some resistive or shearing stresses within the ice or
 198 at the ice-bed interface. For example, when there is a leading-order balance between grav-
 199 itational driving stress (where $\frac{\partial H}{\partial x} \approx \frac{H}{L}$) and basal shear stress set by a Weertman-style
 200 friction law [e.g. $Cu^{\frac{1}{n}}$; Weertman, 1957], the vertically-averaged ice flux is

$$201 \quad Q = \left(\frac{\rho_i g}{C} \right)^n \frac{H^{2n+1}}{L^n}, \quad (10)$$

202 which gives $\alpha = 7$, $\gamma = 3$, and $\nu = \left(\frac{\rho_i g}{C} \right)^n$ for the commonly assumed value of the
 203 Glen’s flow law exponent, $n = 3$. However, if we instead wanted to capture interior ice
 204 flux though vertical shear deformation within the ice column, then we would pick $\alpha = 8$
 205 and $\gamma = 3$ [Cuffey and Paterson, 2010]. By picking such a general form of the interior
 206 ice flux, we admit a wide array of possible choices for the processes driving interior ice
 207 flow. In this study, we use $\alpha = 7$ and $\gamma = 3$ to aid comparison between our simple model
 208 and more complicated models of marine-terminating glacier flow, many of which assume
 209 that ice flows through sliding in the glacier interior [e.g. Schoof, 2007a]. In both cases,
 210 the H and L represent either global or spatially-averaged quantities. The resulting flux
 211 from the interior (Q) represents the scale of interior ice flux that is purely a function of
 212 the large-scale glacier geometry. The advection of ice from upstream occurs through a
 213 spatially-averaged flux, which does not resolve localized anomalies of ice geometry which
 214 may result in localized anomalies of ice flux. In section 6, we further discuss the conse-
 215 quences of such a spatially-averaged ice flux.

216 Ice exits the grounded glacier by discharge through the grounding line or terminus.
 217 Various approximations for the ice flux through the grounding line have been developed,

218 with different assumptions regarding basal friction and controls on ice-shelf buttressing.
 219 However, regardless of particular assumptions, it is generally the case that the flux of ice
 220 through the grounding line or terminus (Q_g) is a function of the local ice thickness (h_g)

$$221 \quad Q_g = \Omega h_g^\beta, \quad (11)$$

222 where β is an exponent that can be derived from asymptotic boundary layer analysis of
 223 the grounding line [Schoof, 2007a; Tsai et al., 2015; Schoof et al., 2017; Haseloff and
 224 Sergienko, 2018], other mathematical approaches [Lingle, 1984; Hindmarsh, 2012] or es-
 225 timated empirically for tidewater glacier termini [Pelto and Warren, 1991]. Ω is a scalar
 226 parameter which incorporates the various factors (besides ice thickness) that can influ-
 227 ence ice flux in the grounding zone or near the terminus. In this study, we primarily (ex-
 228 cept in section 2.2) use two versions of the grounding-line flux derived in Haseloff and
 229 Sergienko [2018], which both assume strong buttressing by an ice shelf. In the limit that
 230 the ice shelf primarily loses mass through calving

$$231 \quad \Omega = (n/2)^n (n+1)^{-(n+1)} \left[\rho_i g (1 - \lambda^{-1}) \right]^n A_g L_s^{-n} W_s^{n+1}, \quad (12)$$

232 where n is the Nye-Glen flow law exponent, A_g is the Nye-Glen flow law coefficient,
 233 L_s is the length of the buttressing ice shelf, and W_s is the width of the ice shelf. In this
 234 grounding-line flux approximation, $\beta = n + 1 = 4$ and thus Q_g has a strongly nonlin-
 235 ear dependence on local ice thickness. In the limit that the ice shelf primarily loses mass
 236 through basal melting

$$237 \quad \Omega = (n+1)^{-\frac{1}{n+1}} \left[\rho_i g (1 - \lambda^{-1}) \right]^{\frac{n}{n+1}} A_g^{\frac{1}{n+1}} W_s \left(-\frac{\dot{m}}{2} \right)^{\frac{n}{n+1}}, \quad (13)$$

238 where \dot{m} is the basal melt rate (with the convention that $\dot{m} < 0$ indicates melting) and
 239 $\beta = 1$. These particular forms of the $Q_g(h_g)$ relationship allow us to understand how
 240 changes in the ice shelf cause changes in the thickness and grounding-line position of a
 241 marine-terminating glacier (see section 4). However, we can equally well use the $Q_g(h_g)$
 242 relationships derived in other studies [Schoof, 2007a; Tsai et al., 2015; Schoof et al., 2017].
 243 This flexibility of assumptions is one of the benefits of using a low-order model.

244 Asymptotic approximations for Q_g are not only valid for steady-state glaciers, but
 245 also describe the leading order time-dependent evolution of a bulk glacier (as in equa-
 246 tion 1) when the grounding region is close to a steady state. This condition will be sat-
 247 isfied most of the time, because the grounding region adjusts on a very fast time scale
 248 when compared to the rest of bulk glacier. Mathematically, these adjustment terms enter

249 as higher order correction terms in the evolution equation of the grounding region [see
 250 for example equation 3.37 in *Schoof, 2007a*]. Indeed, previous studies [*Schoof, 2007b*;
 251 *Drouet et al., 2013*] and section 2.2 of this paper, show that when the ice sheet is reason-
 252 ably close to a steady-state, such quasi-steady approximations to the grounding line flux
 253 compare favorably to high-order numerical models of transient grounding line evolution.
 254 That being said, the very fast adjustment time scale described in *Schoof [2007a]* is not
 255 necessarily resolved by the two-stage model in this study.

256 2.2 Comparison to flowline model

257 In this section, we compare the simulated response of a marine-terminating glacier
 258 to external forcing in our two-stage model with a spatially-extended glacier model. This
 259 comparison is helpful in determining how well the simplified dynamics of the two-stage
 260 model emulate a more complex model in terms of predicting response to a range of dif-
 261 ferent forcing amplitudes and time scales. We use a flowline model [similar to what is
 262 described in *Robel et al., 2014*] with buttressing, a Weertman basal sliding law and fine
 263 horizontal resolution (~100 meters) near the grounding line. Velocity is solved from the
 264 following momentum balance and boundary conditions

$$265 \frac{\partial}{\partial x} \left(2hA_g^{-\frac{1}{n}} \left| \frac{\partial u}{\partial x} \right|^{\frac{1}{n}-1} \frac{\partial u}{\partial x} \right) = \rho_i g h \frac{\partial h}{\partial x} + Cu^m \quad (14)$$

$$266 u(x=0) = 0 \quad (15)$$

$$267 \left[2A_g^{-\frac{1}{n}} h \left| \frac{\partial u}{\partial x} \right|^{\frac{1}{n}-1} \frac{\partial u}{\partial x} \right]_{x=L} = \frac{1}{2} \rho_i g \left(1 - \frac{\rho_i}{\rho_w} \right) \theta h(L)^2, \quad (16)$$

269 where θ is a dimensionless buttressing parameter. In this spatially-extended model, ice
 270 flux is not prescribed at the grounding line, but arises from the formation of the grounding-
 271 zone boundary layer, as described by *Schoof [2007a]*. The ice shelf is not explicitly simu-
 272 lated, but the buttressing effect is reproduced through modification of the stress boundary
 273 condition at the grounding line by buttressing parameters θ [*Schoof, 2007b; Haseloff and*
 274 *Sergienko, 2018*]. Ice thickness changes through advection and surface mass balance,

$$275 \frac{\partial h}{\partial t} + \frac{\partial}{\partial x} (uh) = P, \quad (17)$$

276 and reaches flotation at the grounding line

$$277 h(L) = -\lambda b(L). \quad (18)$$

Parameter	Description	Value
A_g	Nye-Glen Law coefficient ($\text{Pa}^{-n} \cdot \text{s}^{-1}$)	4.22×10^{-25}
b_0	Ice divide bed height (m)	-100
b_x	Prograde bed slope	1×10^{-3}
C	Basal friction coefficient ($\text{Pa} \cdot \text{m}^{-1/n} \cdot \text{s}^{1/n}$)	7.624×10^6
g	Acceleration due to gravity ($\text{m} \cdot \text{s}^{-2}$)	9.81
m	Weertman friction law exponent	1/3
n	Nye-Glen Law exponent	3
\bar{P}	Time-averaged accumulation rate ($\text{m} \cdot \text{yr}^{-1}$)	0.3
σ_P	Accumulation rate variance ($\text{m} \cdot \text{yr}^{-1}$)	0.1
α	Interior ice flux thickness exponent	7
γ	Interior ice flux length exponent	3
θ	Buttressing parameter	0.6
Δt	Time step (yr)	1
ρ_i	Ice density ($\text{kg} \cdot \text{m}^{-3}$)	917
ρ_w	Seawater density ($\text{kg} \cdot \text{m}^{-3}$)	1028

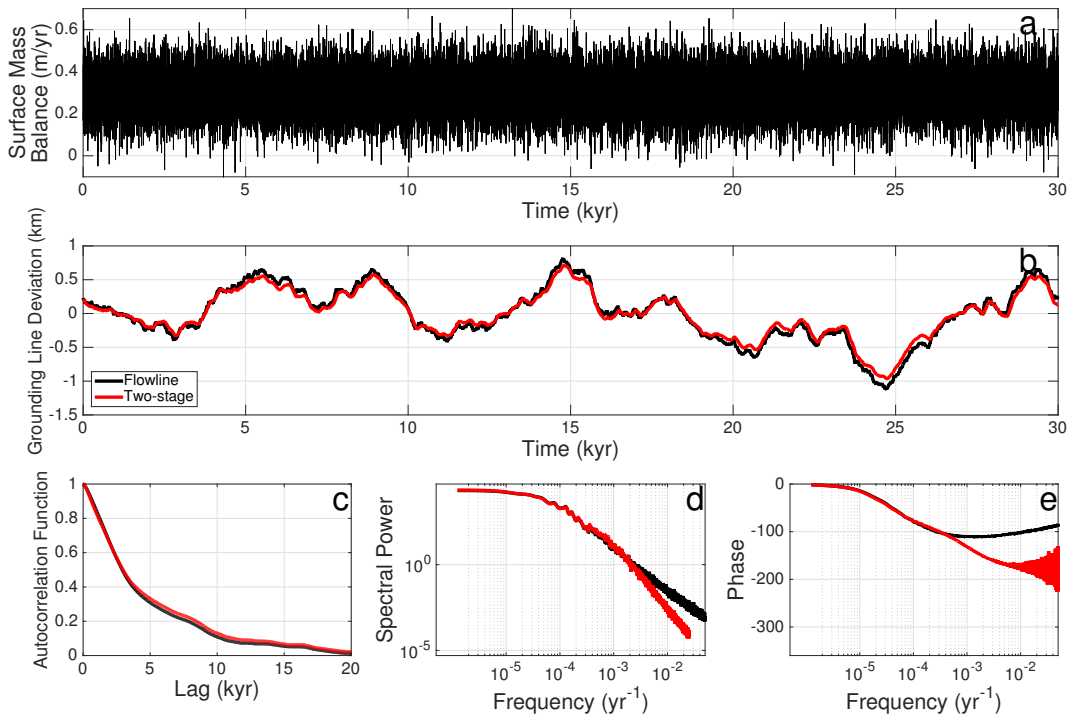
Table 1. Parameters used in comparison simulations in section 2.2.

281

282 This numerical approach has been shown to accurately simulate marine-terminating glacier
 283 velocity and grounding-line dynamics in previous studies [*Schoof*, 2006, 2007b; *Robel*
 284 *et al.*, 2014].

285 To facilitate comparison to this flowline model, we use a grounding line flux ex-
 286 pression in the two-stage model given in *Schoof* [2007a], where $\beta = \frac{m+n+3}{m+1}$ and $\Omega =$
 287 $\left[A_g (\rho_i g)^{n+1} (\theta(1 - \lambda^{-1}))^n (4^n C)^{-1} \right]^{\frac{1}{m+1}}$. We bring both models to a stable equilibrium
 288 state on a downward sloping (prograde) bed, with a constant surface mass balance and
 289 other parameters specified in Table 1. In both the two-stage and flowline models, the re-
 290 sulting equilibrium is a glacier of approximately 2200 m average thickness (H) with a
 291 grounding line 445 km from the ice divide (L). We then perform simulations (Figure 2)
 where stochastic interannual variability (P') is added to the time-averaged surface mass
 balance (\bar{P}). The random year-to-year variations in surface mass balance are drawn from
 a Gaussian normal distribution with mean zero and standard deviation that is 1/3 of the

292 time-average surface mass balance. In both the two-stage and flowline models, we simu-
 293 late the glacier variability forced by the same time series of noisy surface mass balance
 294 (Figure 2a), over 3×10^6 years, to obtain stationary statistical measures of the glacier
 295 variability. These stochastic-forcing simulations are a useful way to sample the response
 296 function for the marine-terminating glacier across a large range of frequencies.



297 **Figure 2.** Comparison between two-stage (red line) and flowline (black line) simulations of grounding-line
 298 variability due to white noise in surface mass balance. (a) Surface mass balance forcing (same for both mod-
 299 els). (b) Simulated grounding-line deviation from stable equilibrium position. 30 kyr time series taken from
 300 a 3000 kyr simulation. (c) Autocorrelation as a function of time lag. (d) Spectral power density as a function
 301 of frequency calculated via Welch's method with a window 1/30 the length of the total time series (10^5 years
 302 in this case). (e) Phase of grounding-line position with respect to forcing in surface mass balance as a function
 303 of frequency.

304 White-noise forcing is the application of random perturbations to a model, drawn
 305 from a Gaussian distribution, and not depending on previous system state or perturba-
 306 tions. White noise forces a system equally at all time scales greater than or equal to the
 307 time scale at which the perturbations are applied. We use such white-noise forcing (Fig-
 308 ure 2a) to perturb the two-stage and flowline glacier systems at every yearly time step,

309 and integrated using the Euler-Maruyama method. Thus, in our system, white noise forces
 310 the glacier at time scales ranging from a year to tens of millennia. Figure 2 compares the
 311 simulated stochastic grounding-line response across these time scales in the flowline model
 312 (black line) and the two-stage model (red line). The two-stage model simulates departures
 313 of the grounding line from its equilibrium position ($y = 0$ in Figure 2b) that are within
 314 10% of the flowline model. Without having to tune any parameters, the structure of the
 315 autocorrelation function, power spectrum and phase (Figure 2c-e) are broadly similar be-
 316 tween the two-stage and flowline models. Perhaps the most notable difference is that the
 317 two-stage model simulates less variability at very short time scales (a few decades) than
 318 the flowline model (Figure 2d). In the flowline model, variability in the surface mass bal-
 319 ance near the grounding zone propagates to the grounding line on time scales of years to
 320 decades and the grounding zone adjusts on a similarly fast time scale [as shown in *Schoof*,
 321 2007a, and discussed in section 2]. Since advection can only occur between the two zones
 322 in the two-stage model (which has a time scale of decades to centuries, see section 3), the
 323 fastest advection time scales are not well represented in the power spectral density and
 324 lagged autocorrelation function of the two-stage model (Figure 2c-d). This lack of vari-
 325 ability at short time scales also leads to a lower standard deviation of fluctuations in the
 326 two-stage model than in the flowline model (by about 20%, see discussion in section 4.3).
 327 Additionally, the phase of the grounding-line response at high frequencies (Figure 2e) is
 328 closer to 180° (indicating surface mass balance forcing precedes the grounding-line re-
 329 sponse) in the two-stage model than the flowline model, which remains between 90° and
 330 120° at these frequencies. The phase of stochastic variations in the flowline model at high
 331 frequencies are the superposition of signals arriving at the grounding line from various
 332 locations throughout the glacier, and thus we should expect the combined grounding-line
 333 response to be less than exactly out of phase (180°). In the two-stage model, the phase
 334 lag of signals at the grounding line are the result of a single advective time scale from the
 335 interior zone to the grounding zone. In practical terms, the two-stage model appears as
 336 a low-pass filter of the flowline model, with small interannual fluctuations in grounding
 337 line positions smoothed out relative to the flowline model. Despite these discrepancies,
 338 it is readily apparent in both models that the amplitude of variability at long time scales
 339 greatly exceeds variability occurring at sub-centennial time scales (Figure 2d). Indeed,
 340 more than 99% of the total variability (measured as the integral over the power spectral
 341 density in Figure 2d) occurs at frequencies in which the two-stage and flowline models are

342 consistent. Consequently, we conclude that the two-stage model successfully emulates the
 343 dynamics which produce the largest amplitude excursions of grounding-line position in the
 344 flowline model.

345 The choice of a two-stage model is also indicated by fitting the time series of sim-
 346 ulated grounding-line position from the flowline model with an autoregressive model of
 347 arbitrary order [the Box-Jenkins method, see *Box et al.*, 2015]. We find that the flowline
 348 model can be well described by a second-order (AR(2)) regressive process governed by
 349 two widely separated time scales, 8300 years and 70 years, for the parameters in Table 1
 350 (and for a range of other parameters, as we will show in section 3). Increasing the number
 351 of stages in the simple model (i.e. an arbitrary AR(p) model with $p > 2$) does improve
 352 the fit to the full flowline model by less than 1% (as judged by the Akaike Information
 353 Criterion for evaluating model quality). However, such an increase in complexity of the
 354 simple model does not improve our understanding of the dynamics of grounding-line vari-
 355 ability and hinders the straightforward analytical characterization of system dynamics that
 356 we describe in the coming sections.

357 **3 Characteristic time scales**

358 A complex numerical model can predict the response of a marine-terminating glacier
 359 to forcing under a variety of assumptions that are specific to that single glacier. Instead,
 360 with a simple model and fewer glacier-specific assumptions, we can derive the generic
 361 response of marine-terminating glaciers to forcing and understand the processes which
 362 control this response. This generic response is characterized by time scales and magni-
 363 tudes of glacier change (or “sensitivities”). A system, such as our two-stage model for a
 364 marine-terminating glacier, that is linearized about a stable equilibrium can be described
 365 more succinctly (and physically) by considering the time scales and sensitivities that gov-
 366 ern the transient response to perturbations away from equilibrium. Such an approach is
 367 considerably more difficult in systems with many degrees of freedom.

368 We start by assuming that the two prognostic variables in the two-stage model, spatially-
 369 averaged ice thickness H , and grounding-line position L , are composed of a stable equilib-
 370 rium state (\bar{H}, \bar{L}) and departures from this state (H', L') that are not necessarily stochastic

371 fluctuations (rather deterministic functions of time)

$$372 \quad H = \bar{H} + H' \quad (19)$$

$$373 \quad L = \bar{L} + L'. \quad (20)$$

374
375 We assume that the departures are small compared to the stable equilibrium states ($H' \ll$
376 \bar{H} , $L' \ll \bar{L}$). We can then substitute these expressions into the two-stage model (equa-
377 tions 7 and 8), expand, and drop all terms that are higher than first order in H' and L'

$$378 \quad \frac{\partial \bar{H}}{\partial t} + \frac{\partial H'}{\partial t} = P - \frac{\bar{Q}_g}{\bar{L}} - \frac{\bar{H}}{\bar{h}_g \bar{L}} (\bar{Q} - \bar{Q}_g) + A_H(\bar{H}, \bar{L})H' + A_L(\bar{H}, \bar{L})L' \quad (21)$$

$$379 \quad \frac{\partial \bar{L}}{\partial t} + \frac{\partial L'}{\partial t} = \frac{1}{\bar{h}_g} (\bar{Q} - \bar{Q}_g) + B_H(\bar{H}, \bar{L})H' + B_L(\bar{H}, \bar{L})L', \quad (22)$$

380
381 where A_H , A_L , B_H and B_L are the strengths of linearized feedbacks in the glacier sys-
382 tem (expressions given in the supporting information). The strengths of these individual
383 feedbacks are a function of the equilibrium glacier state (\bar{H}, \bar{L}). A_H is the magnitude of
384 changes in interior ice flux due to changes in average ice thickness (H). A_L is the mag-
385 nitude of changes in grounding-line ice flux (Q_g) and grounding zone ice-flux difference
386 ($Q - Q_g$) due to changes in grounding-line position (L). B_H is the magnitude of changes in
387 interior ice flux due to changes in grounding line ice thickness ($\frac{Q}{h_g}$). B_L is the magnitude
388 of changes in grounding-zone ice-flux divergence ($\frac{Q - Q_g}{L}$) due to changes in ground-
389 line position (L).

390 When a stable equilibrium exists for a given glacier, $\frac{\partial \bar{H}}{\partial t}$ and $\frac{\partial \bar{L}}{\partial t}$ are by definition
391 zero and the equilibrium terms (not involving departures from equilibrium) on the right-
392 hand side of equations 21 and 22, which reflect the balance of stable equilibrium, sum
393 to zero. This leaves a linear system of equations for departures in ice thickness (H') and
394 grounding-line position (L') and their associated feedbacks

$$395 \quad \frac{\partial H'}{\partial t} = A_H(\bar{H}, \bar{L})H' + A_L(\bar{H}, \bar{L})L' \quad (23)$$

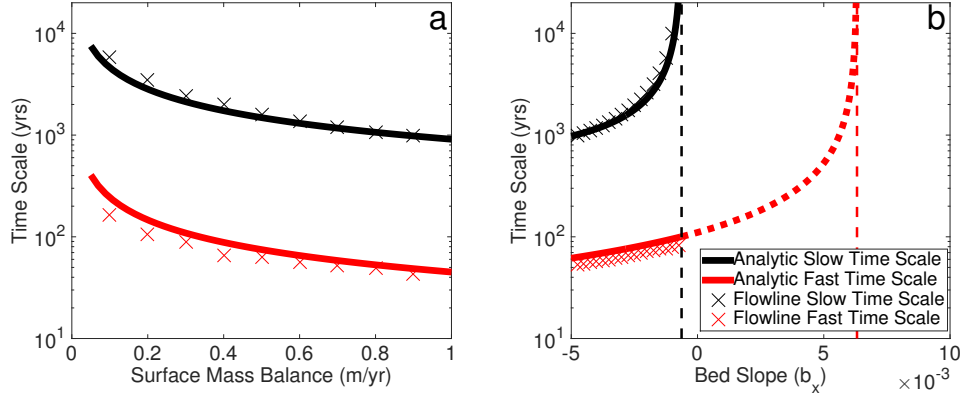
$$396 \quad \frac{\partial L'}{\partial t} = B_H(\bar{H}, \bar{L})H' + B_L(\bar{H}, \bar{L})L'. \quad (24)$$

398 Generally, the solution to such a linear system of equations (23 and 24) is

$$399 \quad L'(t) = C_S e^{-\frac{t}{T_F}} + C_L e^{-\frac{t}{T_S}} \quad (25)$$

400 where the eigenvalues of the system of equations are $-T_F^{-1}$ and $-T_S^{-1}$. These two expo-
401 nential functions correspond to two characteristic time scales of adjustment in the marine-
402 terminating glacier. Put another way, the eigenvalues of the linearized system quantify the

403 adjustment rate and their sign determines the stability of the two-stage model (as in a lin-
 404 ear stability analysis). If at least one of these eigenvalues is positive, there is no stable
 405 equilibrium, causing perturbations to grow rather than dissipate on at least one time scale.
 406 We discuss the nature of this instability in section 3.3.



407 **Figure 3.** Characteristic time scales of the marine-terminating glacier response to external forcing. Thick
 408 lines are analytic predictions of fast (red) and slow (black) time scales from linearized two-stage model (equa-
 409 tions 26 and 27). Crosses are corresponding time scales calculated from an autoregressive-moving-average
 410 (ARMA) fit to flowline model simulations using the Box-Jenkins method [Box *et al.*, 2015]. (a) Varying time-
 411 averaged surface mass balance (\bar{P}). Constant bed slope, $\bar{b}_x = -3 \times 10^{-3}$. (b) Varying bed slope at equilibrium
 412 state (\bar{b}_x). Constant time-averaged surface mass balance, $\bar{P} = 0.5$ m/yr. Black dashed line is the instability
 413 threshold for the slow time scale (equation 33). Thin red dashed line is the instability threshold for the fast
 414 time scale (equation 34). At bed slope greater than the instability threshold for the slow time scale, there is no
 415 longer a stable equilibrium and so a thick dashed red line is based on the analytic prediction of fast time scale
 416 with an unstable fixed point.

417 After some further approximation (detailed in the supporting information), we can
 418 analytically derive the two time scales of the two-stage model

$$419 \quad T_F = \frac{\bar{L}\bar{h}_g}{\bar{Q}(\alpha + \gamma)} - \frac{\bar{h}_g^2}{\bar{Q}_g\beta\lambda\bar{b}_x} \quad (26)$$

$$420 \quad T_S = -\frac{\bar{H}\bar{h}_g\bar{L}^2}{\alpha T_F \bar{Q}} \left[\bar{Q} + \left(\frac{\beta\lambda\bar{b}_x\bar{L}}{h_g} \right) \bar{Q}_g \right]^{-1}. \quad (27)$$

422 We calculate these timescales for a range of values of surface mass balance and bed slope
 423 (Figure 3). In general, there is a slow time scale (T_S) that is one to two orders of mag-
 424 nitude greater than the other time scale (T_F), which we call the fast time scale. For typi-
 425 cal marine-terminating glacier thickness and time-averaged surface mass balance, the fast

426 time scale ranges from decades to centuries and the slow time scale ranges from centuries
 427 to millennia (Figure 3a). Furthermore, as Figure 3 shows, these analytically derived time
 428 scales (solid lines) agree well with those determined from fitting the stochastic variability
 429 simulated in a spatially-extended flowline model (crosses; described in section 2.2) with
 430 an autoregressive model through the Box-Jenkins fitting method [Box *et al.*, 2015]. As we
 431 discuss in section 2.2, there are other, even faster time scales of years to decades that con-
 432 tribute to advective adjustment of the glacier and grounding zone to external forcing and
 433 which are related to the fast adjustment time scale in the asymptotic analyses of *Schoof*
 434 [2007a] and *Haseloff and Sergienko* [2018]. However, as we show these very fast time
 435 scales play a lesser role in setting the transient glacier adjustment to external forcing.

436 3.1 Fast time scale

437 The physical processes that control the fast glacier response to perturbations can
 438 be understood from the form and origin of the terms in T_F (equation 26). The first term
 439 on the right-hand side of equation 26 derives from the interior flux feedback to changes
 440 in ice thickness (A_H), and corresponds to the rate of interior advection (\bar{Q}) of anomalies
 441 in grounding line ice thickness. The second term is the rate at which ice-flux divergence
 442 in the grounding zone changes as the grounding line migrates (B_L). At equilibrium, the
 443 surface mass balance is balanced by interior and grounding-line flux: $\bar{P}\bar{L} = \bar{Q} = \bar{Q}_g$. We
 444 can then simplify the fast time scale as

$$445 T_F = \frac{\bar{h}_g}{\bar{P}} (\alpha + \gamma + 1 - S_T)^{-1}. \quad (28)$$

446 where

$$447 S_T = 1 + \frac{\beta\lambda\bar{b}_x\bar{L}}{\bar{h}_g}, \quad (29)$$

448 is a stability parameter that is typically $O(1)$ and negative for sufficiently prograde bed
 449 slopes (downward sloping in the direction of flow, or $\bar{b}_x < 0$). On prograde slopes ($b_x <$
 450 0) the terms in T_F have the same sign, and so the fast time scale is set by the largest term,
 451 $\alpha + \gamma \approx 10$ (where $\alpha + \gamma \gg \beta\lambda\bar{b}_x\bar{L}\bar{h}_g^{-1}$). This implies that the primary control on the fast
 452 time scale is the rate of advective adjustment of grounding-zone ice thickness. Thus, the
 453 fast time scale may be approximated as

$$454 T_F \approx \frac{\bar{h}_g}{\bar{P}(\alpha + \gamma)}. \quad (30)$$

455 In a stable equilibrium, this rate of advective adjustment is proportional to $\frac{\bar{h}_g}{\bar{P}}$, which is
 456 the “reservoir time scale” on which ice volume in the grounding zone region is replaced

457 by the surface mass balance. Though this approximation is not explicitly dependent on
 458 processes occurring in the ice shelf, their influence does enter through the way in which
 459 they contribute to setting the equilibrium grounding line ice thickness (\bar{h}_g). The reservoir
 460 time scale (generically $\frac{h}{\dot{p}}$) is also discussed in previous studies of the glacier response to
 461 forcing [Nye, 1960, 1963a,b, 1965; Jóhannesson *et al.*, 1989; Harrison *et al.*, 2003], which
 462 found that even if we did not know the glacier velocity or internal dynamics all that well
 463 [as assumed in Harrison *et al.*, 2003], we could use the observed geometry to understand
 464 the glacier sensitivity through this reservoir time scale. Fortunately, recent advances in
 465 grounding-line dynamics have allowed us to explicitly derive the non-dimensional parame-
 466 ter that modifies this reservoir time scale (the unknown parameter f in Jóhannesson *et al.*
 467 [1989] and $\alpha + \gamma \approx 10$ in equation 30). This non-dimensional parameter quantifies how
 468 the particular glacier dynamics may also play a role (in addition to the geometry) in set-
 469 ting the glacier response time scales. In these ways, our approach of studying glacier de-
 470 partures about an equilibrium state explicitly links glacier geometry to ice dynamics, and
 471 allows us to make progress from previous approaches to understanding glacier response
 472 time scales.

473 3.2 Slow time scale

474 The slow glacier response to forcing (equation 27) is a function of the fast time
 475 scale, the magnitude of the interior ice-flux feedback, and the grounding-zone flux-divergence
 476 feedback. At equilibrium, the time-averaged surface mass balance is balanced by interior
 477 and grounding-line flux ($\bar{P}\bar{L} = \bar{Q} = \bar{Q}_g$), and so the slow time scale simplifies to

$$478 T_S = -\frac{\bar{H}\bar{h}_g}{\alpha T_F \bar{P}^2 S_T}. \quad (31)$$

479 When multiplied by the grounding-zone ice flux (Q_g), the stability parameter S_T tracks
 480 the difference between the rates of glacier advective adjustment and extension of the glacier
 481 by grounding-line migration. For typical stable grounding lines (where T_F is approxima-
 482 tion given by equation 30), the slow time scale can be approximated as

$$483 T_S \approx \frac{\bar{H} \left(1 + \frac{\gamma}{\alpha}\right)}{\bar{P} S_T}, \quad (32)$$

484 which is millennia for typical accumulation rates and ice thicknesses (see Figure 3). Phys-
 485 ically, this slow time scale corresponds to the rate at which perturbations in ice thickness
 486 advected into the grounding zone are dissipated by differences in advective and exten-
 487 sional adjustment. The slow time scale includes the reservoir time scale for the entire

488 glacier, $\frac{H}{P}$, though the explicit inclusion of glacier velocity in our model leads to mod-
 489 ification by the stability parameter (S_T) and the interior ice flux exponents (α , γ). As a
 490 result, the slow time scale is longer than the fast time scale by one-to-two orders of mag-
 491 nitude. Indeed this response time of centuries to millennia for stable marine-terminating
 492 glaciers is more similar to that derived numerically in the idealized outlet glacier mod-
 493 eling study of *van der Veen* [2001]. As the bed slope becomes shallower, S_T decreases,
 494 causing the slow time scale to increase, before eventually becoming negative, as we dis-
 495 cuss in the next section.

496 3.3 Instabilities of time scales

497 *Weertman* [1974] first established that ice sheet grounding lines are unstable on ret-
 498 rograde bed slopes (upward sloping in the direction of flow, or $\bar{b}_x > 0$), commonly re-
 499 ferred to as the “marine ice sheet instability”. Subsequent work has found that this in-
 500 stability extends to flat and shallow prograde beds [*Schoof*, 2012], though other factors
 501 may play a role in modulating this stability threshold in bed slope [*Gomez et al.*, 2010;
 502 *Jamieson et al.*, 2012; *Gudmundsson et al.*, 2012] and the rate of grounding line migra-
 503 tion under instability [*Brondey et al.*, 2017]. In our model, this instability occurs when the
 504 slow time scale becomes negative ($-1/T_S \geq 0$ in equation 25) as bed slope flattens (b_x is
 505 negative and increasing) and S_T becomes positive. This happens at

$$506 \quad \bar{b}_x^{*S} = -\frac{\bar{h}_g}{\beta\lambda\bar{L}}, \quad (33)$$

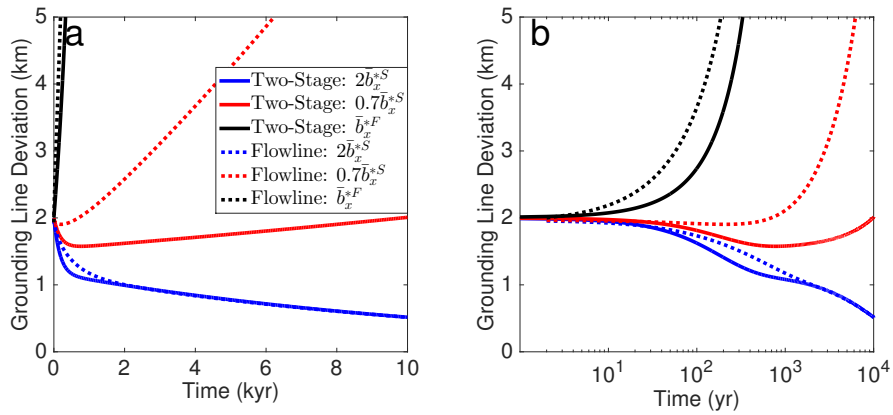
507 which corresponds to a shallow prograde bed slope (black dashed line in Figure 3b). Ex-
 508 actly at this stability threshold, the slow time scale diverges, which physically corresponds
 509 to a glacier at neutral stability where perturbations to glacier state are neither damped or
 510 amplified by the glacier response (on this slow time scale). This stability threshold is also
 511 consistent with the linear stability condition derived by *Schoof* [2012], in which grounding
 512 lines resting on retrograde and shallow prograde bed slopes are unstable to perturbations.
 513 We have written the stability criterion as a function of equilibrium glacier geometry [in-
 514 stead of surface mass balance, as in *Schoof*, 2012], which is, in part, set by the surface
 515 mass balance ($P\bar{L} = \bar{Q}_g$). Past this threshold in bed slope, the slow time scale is no longer
 516 defined since the stable equilibrium glacier state no longer exists.

517 Conversely, the fast time scale remains finite and defined for bed slopes flatter and
 518 more retrograde than \bar{b}_x^{*S} . The fast time scale increases until it also diverges ($T_F \rightarrow \infty$)

519 and then become negative at a moderately steep retrograde slope of

$$520 \quad \bar{b}_x^{*F} = \frac{\bar{h}_g}{\beta \lambda \bar{L}} (\alpha + \gamma). \quad (34)$$

521 Above this threshold, the decay rate associated with the fast time scale is positive ($-1/T_F \geq$
 522 0 in equation 25). As bed slope increases, changes in grounding-line position cause less
 523 adjustment through grounding-line flux (i.e. the third term on the right-hand side of equa-
 524 tion 26 decreases in magnitude). Eventually, perturbations in the grounding line position
 525 can no longer be accommodated by changes in ice advection to the grounding zone and
 526 the fast time scale becomes negative.



527 **Figure 4.** Grounding-line migration from an initially perturbed state (2 km from equilibrium) simulated
 528 in two-stage (solid lines) and flowline (dashed lines) models for a range of bed slopes at the grounding line.
 529 The blue line is the stable grounding line response for a prograde bed slope steeper than the slow stability
 530 threshold ($\bar{b}_x = -5.1 \times 10^{-4}$). The red line is the grounding line response for a prograde bed slope shallower
 531 than the slow stability threshold ($\bar{b}_x = -1.8 \times 10^{-4}$). The black line is the unstable grounding line response
 532 for a retrograde bed slope at the fast stability threshold ($\bar{b}_x^{*F} = 2.6 \times 10^{-3}$). (a) Plotted in linear coordinates.
 533 (b) Plotted with logarithmic coordinates on the x-axis.

534 It is always the case that $\bar{b}_x^{*S} < \bar{b}_x^{*F}$, or that as bed slope becomes shallower, slow
 535 grounding-line dynamics become unstable before fast grounding-line dynamics. This im-
 536 plies that there is a wide range of intermediate shallow bed slopes ($\bar{b}_x^{*S} < \bar{b}_x < \bar{b}_x^{*F}$, the
 537 region between the thin black and red dashed lines in Figure 3b) for which the ground-
 538 ing line is unstable on slow time scales, but stable on fast time scales. We demonstrate
 539 the consequence of these distinct stability thresholds in Figure 4, which shows two-stage
 540 (solid) and flowline (dashed) model simulations of the grounding-line migration from an

541 initially perturbed state (2 km) for several different bed slopes. A grounding line on a
 542 steep prograde bed slope (blue lines, for which $\bar{b}_x < \bar{b}_x^{*S}$) exhibits stable dissipative behav-
 543 ior (i.e. it returns to equilibrium) at both short and long time scales. For strongly retro-
 544 grade bed slopes (black lines, for which $\bar{b}_x = \bar{b}_x^{*F}$), the grounding line is unstable on both
 545 fast and slow time scales. In such a scenario, even short-lived departures in the glacier
 546 state from equilibrium immediately grow, rather than decay. For shallow prograde or shal-
 547 low retrograde bed slopes (red lines, for which $\bar{b}_x^{*S} < \bar{b}_x < \bar{b}_x^{*F}$) the perturbed grounding-
 548 line position is nearly stagnant or retreating towards equilibrium (at $y = 0$) on fast time
 549 scales (centuries), but is unstable on long time scales (millennia). When the grounding
 550 line is unstable and the glacier is strongly out of equilibrium, asymptotic approximations
 551 for the grounding line flux (equation 11) become less accurate [*Schoof, 2007b*]. This is
 552 apparent from the increasing departure between the unstable retreat simulated in the flow-
 553 line and the two-stage model on time scales of millennia. Nonetheless, both models indi-
 554 cate that there is a range of bed slopes for which a perturbed grounding line may exhibit
 555 stable behavior on the short term, but is ultimately unstable in the long term. This non-
 556 monotonic grounding line response to a perturbation occurs because marine-terminating
 557 glaciers have more than one time scale both in the two-stage and flowline models, which
 558 become unstable at different bed slope thresholds. We call this scenario, when the slow
 559 time scale is unstable, but the fast time scale is stable, the “slow” marine ice sheet insta-
 560 bility. For sufficiently steep retrograde slopes the grounding line is unstable at both slow
 561 and fast time scales. We call this the “fast” marine ice sheet instability.

562 Many glaciers in Greenland and West Antarctica are (likely) undergoing an unsta-
 563 ble retreat over steep retrograde bed slopes at rates of kilometers per year [*Joughin et al.*,
 564 2008; *Park et al.*, 2013; *Scheuchl et al.*, 2016]. In this section, we determined the condi-
 565 tions under which this instability occurs (equations 34 and 33), and show qualitatively that
 566 rapid glacier change may occur due to the “fast” marine ice sheet instability. However, we
 567 cannot easily extend our linear analysis of marine-terminating glacier response to quantita-
 568 tively determine the transient rate of glacier change on retrograde or shallow prograde bed
 569 slopes since the lack of a stable equilibrium causes the linearity of the glacier response to
 570 be a bad approximation. Future work may consider using non-equilibrium approaches for
 571 systems near instabilities [*Suzuki, 1977; Nicolis and Nicolis, 1981*] to assess the behavior
 572 of marine-terminating glaciers on retrograde bed slopes.

4 Sensitivity to forcing

Observations indicate that marine-terminating and tidewater glaciers are undergoing strongly heterogeneous changes [Post and Motyka, 1995; Csatho et al., 2014; Felikson et al., 2017; Brinkerhoff et al., 2017]. This heterogeneity may be caused by factors that vary from one glacier to another, such as forcing rate, glacier state, bed topography, or time scale of response. Our challenge is to understand how the magnitude and rate of the glacier response to external forcing is controlled by these various factors. Having derived the characteristic glacier response time scales, we have already solved half the problem of the time-dependent glacier response to forcing. In this section, we will solve the second half of the problem, by deriving the total and transient sensitivity of marine-terminating glacier state to different types of external forcing.

4.1 Total fractional sensitivity

In this section, we derive the sensitivity of marine-terminating glaciers to forcing by extending the linearization of the two-stage model to time-dependent perturbations in external forcing parameters. To demonstrate the approach, we start by decomposing P (the spatially-averaged surface mass balance) into time-averaged and perturbed components

$$P = \bar{P} + P' \quad (35)$$

which leads to an expanded forms of linear equation 23

$$\frac{\partial H'}{\partial t} = A_H(\bar{H}, \bar{L})H' + A_L(\bar{H}, \bar{L})L' + P' \quad (36)$$

which now includes glacier feedbacks to perturbations in surface mass balance. For a change in surface mass balance (P'), we calculate the magnitude of changes in glacier state (H' and L') once the system has reached a new steady state, which occurs when $\frac{\partial H'}{\partial t} = 0$ and $\frac{\partial L'}{\partial t} = 0$ in equations 24 and 36 (derived in detail in supporting information)

$$\frac{H'}{\bar{H}} = \frac{1}{\alpha S_T} \left(\frac{\beta \lambda \bar{b}_x \bar{L}}{\bar{h}_g} - \gamma \right) \frac{P'}{\bar{P}} \quad (37)$$

$$\frac{L'}{\bar{L}} = -\frac{1}{S_T} \frac{P'}{\bar{P}}. \quad (38)$$

These are the fractional sensitivities of average glacier thickness (H'/\bar{H}) and grounding line position (L'/\bar{L}), to a fractional change in surface mass balance (P'/\bar{P}).

We can also derive the glacier sensitivity to changes in the observable ice shelf parameters that go into Ω . For a glacier strongly buttressed by an ice shelf that primarily loses ice through calving (Ω in equation 12), we derive the fractional glacier sensitivity to a fractional change in the ice-shelf length (L'_s/\bar{L}_s)

$$\frac{H'}{\bar{H}} = -\frac{(\gamma + 1)n}{\alpha S_T} \left(\frac{L'_s}{\bar{L}_s} \right) \quad (39)$$

$$\frac{L'}{\bar{L}} = -\frac{n}{S_T} \left(\frac{L'_s}{\bar{L}_s} \right). \quad (40)$$

These sensitivities show the extent of grounding-line retreat and interior ice thinning that would be expected after, for example, the detachment of an iceberg from an ice shelf that reduces the buttressing ice-shelf length (assuming all parts of the ice shelf contribute equally to buttressing). Alternately, we consider an ice shelf that strongly buttresses a glacier and loses mass entirely through basal melting (Ω in equation 13). We then derive the fractional glacier sensitivity to fractional changes in basal melt rate (where $\dot{m} < 0$ indicates melting)

$$\frac{H'}{\bar{H}} = \frac{(\gamma + 1)n}{\alpha(n + 1)S_T} \left(\frac{\dot{m}'}{\bar{\dot{m}}} \right) \quad (41)$$

$$\frac{L'}{\bar{L}} = \frac{n}{(n + 1)S_T} \left(\frac{\dot{m}'}{\bar{\dot{m}}} \right). \quad (42)$$

The fractional sensitivities of ice thickness and grounding-line position (equations 37-42) indicate some general rules about the expected magnitude of the glacier response to external forcing. The fractional change in glacier state from equilibrium can be approximated as proportional to the fractional change in climate forcing ($\frac{P'}{\bar{P}}, \frac{\dot{m}'}{\bar{\dot{m}}}$) or a property of the buttressing ice shelf ($\frac{L'_s}{\bar{L}_s}$). This proportionality is generally modulated by the inverse of the stability parameter (S_T), and the strength of the nonlinearity of the forcing process (1 for surface mass balance, $-n$ for ice shelf length in equation 12 and $\frac{n}{n+1}$ for basal melting rate in equation 13). For ice thickness, the strength of the nonlinearity in interior ice flux (α, γ) also enters. As the bed slope becomes shallower, S_T decreases in magnitude, and a given magnitude of external forcing will result in a larger change in glacier thickness and grounding-line position.

We consider an illustrative example of a marine-terminating glacier that is $\bar{L} = 200$ km long, $\bar{h}_g = 1000$ m thick at the grounding line, and undergoes a 5% decrease in surface mass balance. Using equation (38) we would predict that on a prograde bed slope of $\bar{b}_x = -3 \times 10^{-3}$, the glacier would retreat by 3% of its length. However, if the prograde bed slope is twice as shallow ($\bar{b}_x = -1.5 \times 10^{-3}$) the glacier would instead retreat by 14%

635 of its length, albeit over a longer time scale. Alternately, for the same glacier, a 5% de-
 636 crease in buttressing ice shelf length causes the glacier to retreat by 9% of its length on a
 637 $\bar{b}_x = -3 \times 10^{-3}$ prograde slope and 43% of its length on a $\bar{b}_x = -1.5 \times 10^{-3}$ prograde
 638 slope. The nonlinear dependence of the grounding line flux on ice shelf length leads to a
 639 more sensitive response to perturbations than is the case for perturbations in surface mass
 640 balance.

641 Overall, the sensitivities we derive depend only on glacier state, nonlinearity in
 642 glacier dynamics, and the time-averaged value of the forcing parameter. The magnitude of
 643 grounding line changes on the slow time scale alone can also be simulated by a one-stage
 644 counterpart of the two-stage model of this study (where we assume that $PL = Q$):

$$645 \quad \frac{\partial L}{\partial t} = \frac{1}{h_g} (PL - Q_g). \quad (43)$$

646 Equilibrium occurs when surface mass balance is balanced by grounding line flux ($\bar{P}\bar{L} =$
 647 \bar{Q}_g). Since a change in surface mass balance must be balanced by a change in grounding
 648 line flux, the sensitivity of the grounding-line position will be the same in our two-stage
 649 model, its one-stage counterpart (equation 43), and a range of higher-order models. In-
 650 deed, we find the sensitivities derived in this section match those calculated in the flowline
 651 model described in section 2.2, to the extent that its modeled steady-state grounding line
 652 flux matches the grounding line flux expression used in the two-stage model (equation 11).
 653 We similarly expect that other high-order models that accurately simulate grounding line
 654 flux will also match these sensitivities. In this way, these expressions for glacier sensitivity
 655 serve as useful first-order approximations for the glacier response that can be calculated
 656 without use of a complex ice-sheet model.

657 **4.2 Transient response to trends and step changes in forcing**

658 The glacier response to forcing is not instantaneous, but rather evolves in time. In
 659 this section we derive the transient grounding line migration in response to a trend or step
 660 change in external forcing. We then discuss the relative importance of forcing rate and the
 661 characteristic time scales in determining the rate of the glacier response to forcing.

We assume that the marine-terminating glacier begins at stable equilibrium with initial conditions

$$L'(t = 0) = 0 \quad (44)$$

$$\left. \frac{dL'}{dt} \right|_{t=0} = 0. \quad (45)$$

We then apply a trend (\dot{P}) in surface mass balance (though the same general approach applies for a trend in any parameter), $P'(t) = \dot{P}t$. We solve for the time-dependent grounding line position in equations 36 and ?? (linearized form of the two-stage model) using the method of undetermined coefficients (complete derivation in supporting information)

$$L'(t) = \dot{P}L_P T_S \left[\frac{1}{2} \left(1 - \frac{T_S - 2T_F}{(T_S^2 - 4T_S T_F)^{\frac{1}{2}}} \right) e^{-\frac{t}{T_F}} + \frac{1}{2} \left(1 + \frac{T_S - 2T_F}{(T_S^2 - 4T_S T_F)^{\frac{1}{2}}} \right) e^{-\frac{t}{T_S}} - 1 + \frac{t}{T_S} \right], \quad (46)$$

where $L_P = -\frac{\bar{L}}{S_T \dot{P}}$ is the grounding-line sensitivity to perturbations in surface mass balance (which can be derived for other parameters from equations 38, 40, 42). This solution is valid when $T_S > 4T_F$, which is true for a range of glacier conditions (Figure 3).

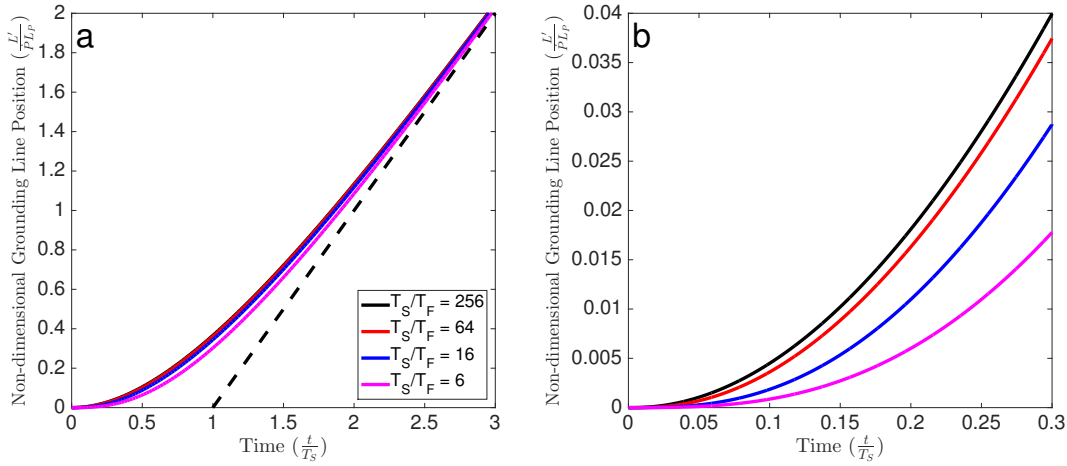


Figure 5. Response of grounding-line position to a trend in surface mass balance (equation 46) for different ratios between fast and slow time scales (T_S/T_F). Grounding line position (y-axis) is non-dimensionalized with $L'/\dot{P}L_P$. Time (x-axis) is also non-dimensionalized with $\frac{t}{T_S}$. (a) Shape of grounding-line trend. Dashed black line is the long term rate of grounding-line migration forced by a trend in surface mass balance (equation 48). (b) Zoomed version of panel (a), meant to highlight the different initial responses to a trend on the fast glacier time scale (T_F).

The transient grounding-line evolution forced by a linear trend in surface mass balance and simulated in the flowline model is well approximated by equation 46 (not plot-

ted). In Figure 5, we show that the shape of the glacier response only depends on the slow and fast time scales, when normalized by the trend rate in forcing and the sensitivity to forcing in a specific parameter ($\dot{P}L_P$). Since typically the slow time scale is much longer than the fast time scale (again, see Figure 3), we can make the simplification that the transient grounding-line response to a trend is only dependent on the slow time scale

$$L'(t) = -\dot{P}L_P T_S \left[e^{-\frac{t}{T_S}} - 1 + \frac{t}{T_S} \right]. \quad (47)$$

Figure 5 shows that as T_S/T_F increases, the transient response converges quickly to this simplified response that only depends on the slow time scale.

After a sufficiently long period of time, the grounding line evolves at a constant rate set by the trend in forcing and the sensitivity (black dashed line in Figure 5a)

$$\left. \frac{\partial L'}{\partial t} \right|_{t \gg T_S} = -\dot{P}L_P. \quad (48)$$

However, the grounding-line migration rate remains relatively small in the time immediately after the onset of a trend (t), as long as $t \ll T_S$ (Figure 5b). Any reasonable estimate of T_S for a marine-terminating outlet glacier in Greenland or Antarctica will be at least 1000 years (Figure 3), whereas the onset of significant anthropogenic forcing trends is estimated to be around 1880 [IPCC, 2013]. This implies that the current stable glacier changes being observed (not including unstable glacier retreat over retrograde slopes, which are discussed in section 3.3) are still close to the onset of the response functions in Figure 5. Hence, the initial glacier retreat over a prograde bed that is caused by industrial-era trends in climate occurs at an approximate rate,

$$\left. \frac{dL'}{dt} \right|_{t \ll T_S} \approx -\dot{P}L_P \frac{t}{T_S}, \quad (49)$$

that is a small fraction ($\frac{t}{T_S}$) of the long-term grounding-line migration rate expected from a continuation of the industrial-era trend in climate forcing (equation 48). Put another way, if current rates of climate change continue, we would expect that the grounding-line migration rate of stable marine-terminating glaciers will eventually accelerate to be many times (perhaps even an order of magnitude if $T_S > 1000$ years) greater than current rates, even if the grounding line does not migrate into regions of retrograde or drastically different bed slope.

The response of the grounding line to a step change in forcing (of magnitude P') is similarly straightforward to derive, from equations (36), (??) and initial conditions (44)

713 and (45), the transient solution is

$$714 \quad L'(t) = -L_P P' \left[\left(\frac{T_F}{T_S - T_F} \right) e^{-\frac{t}{T_F}} - \left(\frac{T_S}{T_S - T_F} \right) e^{-\frac{t}{T_S}} + 1 \right], \quad (50)$$

715 with the fast and slow adjustment time scales mediating the grounding-line response.

716 Observational records of marine-terminating glacier thickness and length tend to be
 717 short. Though reconstructions of local climate may be longer, climate trends can often be
 718 difficult to accurately estimate in the presence of inter- and sub-annual climate variabil-
 719 ity. This inability to precisely determine when a trend started can make it difficult to ex-
 720 actly pinpoint when a change in forcing begins (i.e., when $t = 0$ in equations 46 and 50).
 721 Consequently, uncertainty in the time of climate forcing onset ($t = 0$) leads to significant
 722 uncertainty in short- to medium-term projections of marine-terminating glacier change.

723 4.3 Stochastic variability

724 Stochastic variability of marine-terminating glaciers will arise in the presence of in-
 725 ternal variability in climate forcing. To identify the response of glaciers to climate changes,
 726 it is first necessary to understand the response of glaciers to stochastic climate variability.
 727 In this study, we consider white-noise perturbations in forcing parameters.

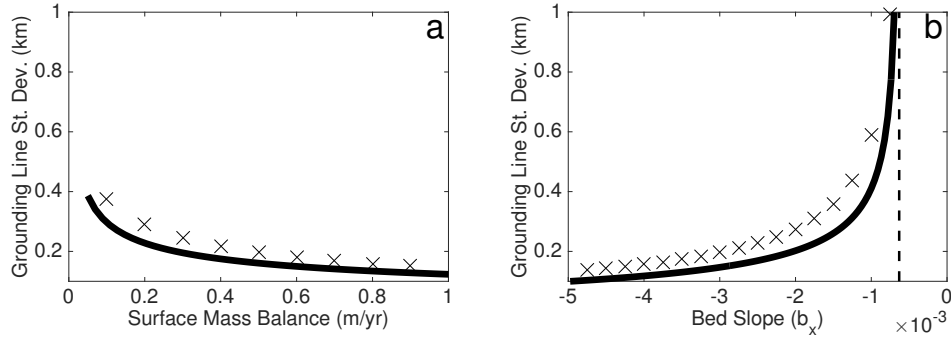
728 The linearized two-stage model equations (36-??) are discretized in time using a for-
 729 ward Euler-Maruyama method, implying an Itô formulation of the stochastic differential
 730 equation. Combining the two discretized equations, we derive a second-order autoregres-
 731 sive (AR(2)) model for the grounding-line position

$$732 \quad L_t = \left(2 - T_F^{-1} \Delta t - T_F^{-1} T_S^{-1} \Delta t^2 \right) L_{t-\Delta t} + \left(-1 + T_F^{-1} \Delta t \right) L_{t-2\Delta t} - T_F^{-1} T_S^{-1} \Delta t^2 L_P P', \quad (51)$$

733 where P' is a Gaussian, white-noise process representing stochastic variability in surface
 734 mass balance at time scale Δt (throughout this study, we take $\Delta t = 1$ year). We then use
 735 the analytic variance of an AR(2) process found in *Box et al.* [2015] to derive the variance
 736 of the grounding-line position. After some approximation (detailed in supporting informa-
 737 tion), the variance of the grounding-line position can be expressed as

$$738 \quad \sigma_L^2 = \frac{T_S \Delta t}{2} \left[\frac{\alpha T_F \bar{P} \bar{L}}{\bar{H} \bar{h}_g} \right]^2 \sigma_P^2 \quad (52)$$

739 where σ_P is the variance of the surface mass balance. All details of the above derivation
 740 are given in the supporting information.



741 **Figure 6.** Standard deviation of grounding-line position fluctuations in response to white noise forcing in
 742 spatially-averaged surface mass balance ($\sigma_P = 0.1$ m/yr). Solid lines are analytic predictions of standard
 743 deviation of grounding-line position (σ_L) from linearized two-stage model (equation 52). Crosses are corre-
 744 sponding standard deviation calculated from flowline model simulations forced with white noise (e.g. Figure
 745 2). (a) Varying time-averaged surface mass balance (\bar{P}). Constant bed slope, $\bar{b}_x = -3 \times 10^{-3}$. (b) Varying bed
 746 slope at equilibrium state (\bar{b}_x). Constant time-averaged surface mass balance, $\bar{P} = 0.5$ m/yr. Black dashed
 747 line is the instability threshold for the slow time scale (equation 33).

748 For a typical marine-terminating glacier in Greenland, $\bar{H} \sim 1$ km, $\bar{Q}_g / \bar{h}_g \sim 1$ km/yr,
 749 $T_S \sim 1000$ yr and $T_F \sim 50$ yr (Figure 3) and interannual variability in surface mass balance
 750 (σ_P) is in the range 0.1 – 1 m/yr [Fyke *et al.*, 2014]. These parameters suggest a range of
 751 $\sigma_L \approx 0.1 - 5$ km. This range is comparable to the few estimates that have been made of
 752 natural marine-terminating glacier variability [e.g., Björk *et al.*, 2012; Hogg *et al.*, 2016,
 753 though such estimates are typically made from short photographic or satellite records].
 754 It should also be noted that noisy forcing with interannual persistence (e.g., red noise)
 755 results in enhanced stochastic glacier variability [Roe and Baker, 2016; Mantelli *et al.*,
 756 2016], and so noise autocorrelation is important to consider when interpreting observa-
 757 tions of glacier variability. Figure 6 demonstrates that, even with the simplifications inher-
 758 ent in the derivation of an analytic approximation of grounding-line variability (solid line),
 759 equation (52) agrees with numerically calculated grounding line variability from a flow-
 760 line model (crosses) to within 20%. The analytic prediction is systematically below the
 761 flowline model because, the two-stage model has muted fluctuations at high-frequencies
 762 compared to the flowline model (though these high frequency fluctuations typically have
 763 amplitude < 100 m, see Figure 2b and section 2.2).

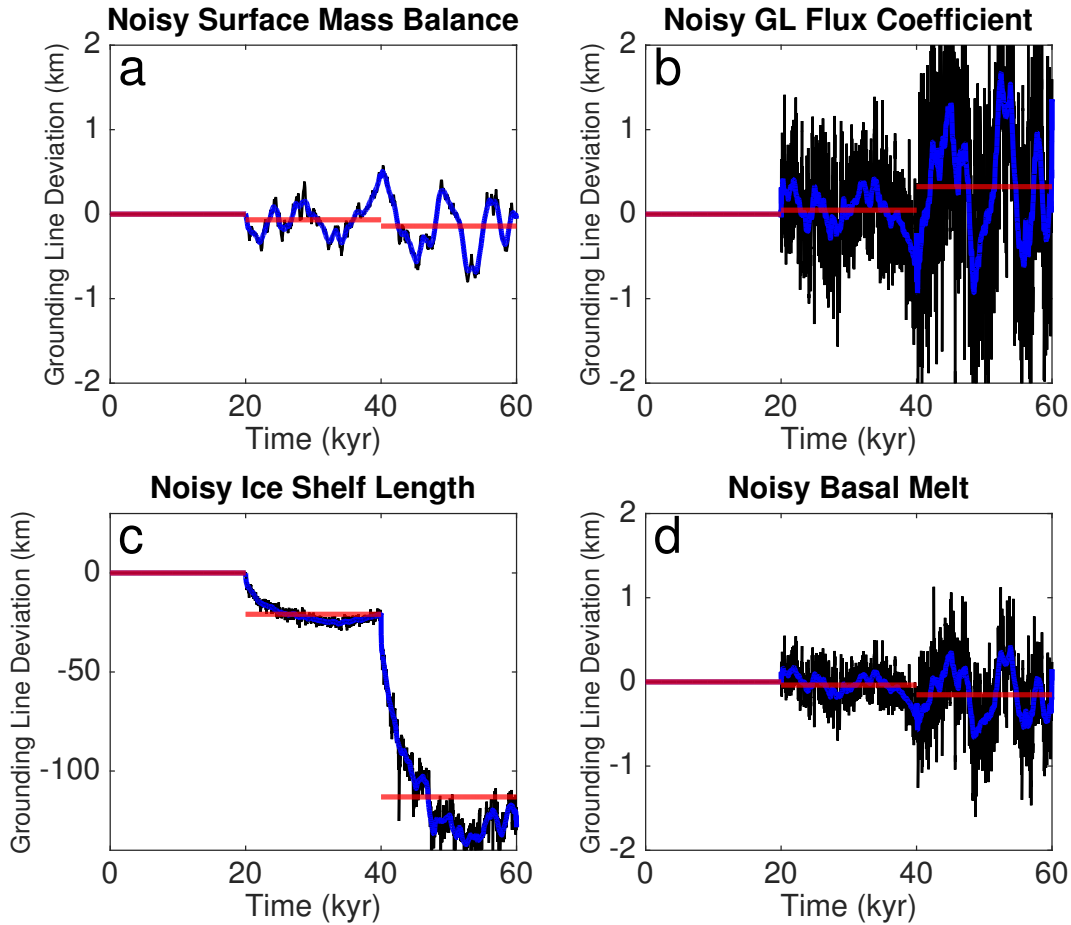
764 Stochastic grounding line variability (equation 52) is dependent on both the short
 765 and fast time scales. Thus, as bed slopes become shallower and approach the slow time-
 766 scale instability (equation 33), the variance of grounding-line position increases rapidly
 767 along with the slow time scale (Figure 6b). This increasing variance and decreasing rate
 768 of dissipation of fluctuations are hallmarks of “critical slowdown”, which is a generic fea-
 769 ture of dynamical systems smoothly approaching bifurcations to instability [e.g., *Lenton,*
 770 2011].

771 **5 Nonlinearity of noisy processes causes grounding-line retreat**

772 In our two-stage model of a marine-terminating glacier, noise in surface mass bal-
 773 ance (P') is additive because it directly perturbs the glacier thickness, but does not depend
 774 on the glacier state. On the other hand, noise in the coefficient of grounding-line flux (Ω')
 775 is multiplicative because it perturbs the grounding-line flux, which also depends on the
 776 grounding-line position. In this section, we show that nonlinearity in a multiplicative noise
 777 process changes the time-averaged equilibrium state of a marine-terminating glacier.

778 In Figure 7, we compare the response of the two-stage glacier model to white-noise
 779 forcing in four different environmental parameters: surface mass balance (P), coefficient
 780 of grounding-line flux (Ω), ice-shelf length (L_s) and basal melt (\dot{m}). In each of these 60
 781 kyr simulations, we simulate the grounding-line response to forcing without noise in the
 782 first 20 kyr, with white noise of magnitude equal to 10% of the mean in the next 20 kyr,
 783 and with white noise of magnitude equal to 20% of the mean in the final 20 kyr. As we
 784 have seen previously in this study, when there is white noise in the spatially-averaged sur-
 785 face mass balance (Figure 7a), the time-averaged grounding-line position remains constant
 786 regardless of the magnitude of noise.

795 We also vary the magnitude of noise in the coefficient of grounding-line flux (Ω' ;
 796 Figure 7b). However, even though this is a multiplicative noise process, the time-averaged
 797 glacier state does not appear to depend significantly on the magnitude of the noise. This
 798 is because the state variable in the grounding-line flux term, h_g , does not strongly vary
 799 when ice is thick at the grounding line, leading to rather weak state-dependence. If instead
 800 ice was thinner at the grounding line (such as in a tidewater glacier), grounding line flux
 801 would be more sensitive to small changes in system state, thus leading to stronger state-
 802 dependence.



787 **Figure 7.** Grounding-line deviation from equilibrium simulated in the two-stage model due to noise in
 788 different forcing parameters. Black line in all panels is year-to-year grounding-line position simulated in
 789 two-stage model. Blue line is 1000-year running average. Red line in all panels is average over time period of
 790 constant noise magnitude. 0-20 kyr in all simulations have no noise in forcing. 20-40 kyr in all simulations
 791 have noise with standard deviation equal to 10% of mean forcing value. 40-60 kyr in all simulations have
 792 noise with standard deviation equal to 20% of mean forcing value. (a) Noise in surface mass balance (P'). (b)
 793 Noise in grounding-line flux coefficient (Ω'). (c) Noise in ice-shelf length (L'_s). (d) Noise in ice-shelf basal
 794 melt (m').

803 In reality, noise does not occur in Ω directly, but rather in the various processes that
 804 contribute to Ω . The grounding-line flux of a glacier buttressed by a calving-dominated
 805 ice shelf is a function of L_s^{-n} (equation 12). We consider a scenario where the calving of
 806 icebergs from an ice shelf causes white-noise fluctuations in L_s [Bassis, 2011]. The corre-
 807 sponding time-averaged grounding-line position (Figure 7c, note the different y-axis scale)
 808 is strongly a function of the magnitude of the forcing. Of all the forcing processes con-

809 sidered here, this shift in the time-averaged state is by far the largest (by more than two
 810 orders of magnitude). We can explain why this shift occurs by noting that when ice-shelf
 811 length increases from its equilibrium value by 10%, grounding-line flux decreases by 25%
 812 and when ice-shelf length decreases from its equilibrium value by 10%, grounding-line
 813 flux decreases by 37%. Thus, though the distribution of noisy ice-shelf length is symmet-
 814 ric, the corresponding distribution of noisy grounding-line flux is asymmetric, leading to a
 815 shift in the time-averaged grounding-line flux and glacier state. Though we have assumed
 816 that the noise forcing of ice-shelf length includes no persistence in time (white noise), it
 817 would be more realistic to simulate ice shelf calving with autocorrelation in time. This
 818 would lead to greater stochastic glacier variability [Roe and Baker, 2016; Mantelli et al.,
 819 2016] and perhaps an even larger shift in the time-averaged glacier state.

820 Such a dependence of the mean state on the magnitude of noise forcing is typically
 821 termed “noise-induced drift” and has been explored extensively [e.g., Penland, 2003].
 822 Noise-induced drift has also been noted previously in other nonlinear glacier models with
 823 other types of forcing [Hindmarsh and Le Meur, 2001; Mikkelsen et al., 2017]. Our simu-
 824 lation of noisy calving-induced drift suggests that the character of calving events (i.e. size
 825 and recurrence time) may have a strong influence on the time-averaged glacier state. Con-
 826 sequently, ice sheet models may be strongly biased by parameterizing calving as a deter-
 827 ministic flux or by misrepresenting the nature of calving-induced noise in ice shelf length.
 828 Flexible stochastic approaches to simulate calving, such as Bassis [2011], are better suited
 829 to capturing the noise-induced retreat that we have identified here.

830 *Haseloff and Sergienko* [2018] have also derived a more general relationship between
 831 flux and ice thickness at the grounding line

$$832 \quad \dot{m}\Omega^{\frac{1}{n}}L_s h_g^{\frac{n+1}{n}} = (Q_g + \dot{m}L_s)^{\frac{n+1}{n}} - Q_g^{\frac{n+1}{n}} \quad (53)$$

833 which includes the effect of both sub-ice shelf basal melting and ice-shelf length on but-
 834 tressing. We use this formula to find the grounding-line flux in the presence of interannual
 835 noise in the ice-shelf basal melt [similar to what is predicted by ocean models, e.g. *Schod-*
 836 *lok et al.*, 2012; *Sciascia et al.*, 2013]. We find that the white noise in basal melt has only
 837 a small effect on the time-average grounding-line position (Figure 7d). This is likely due
 838 to the much weaker nonlinearity in basal melt rate ($\frac{n+1}{n} = \frac{4}{3}$).

6 Discussion

6.1 Observed marine-terminating glacier change

Observations indicate that many marine-terminating glaciers have retreated and thinned over the last several decades [Pritchard *et al.*, 2009; Joughin *et al.*, 2010; Moon *et al.*, 2015; Wouters *et al.*, 2015; Scheuchl *et al.*, 2016]. However, there are large glacier-to-glacier variations in recent changes. Even adjacent glacier that have experienced similar rates of ocean and atmospheric warming, have not retreated and thinned uniformly [Larsen *et al.*, 2016; Motyka *et al.*, 2017]. In this study, we have shown that the response of glacier thickness to surface mass balance and ocean forcing (section 4.1) becomes weaker for steeper prograde bed slopes. These findings are in agreement with Felikson *et al.* [2017], who show that almost all thinning observed at marine-terminating glaciers in West Greenland occurs downstream of steep regions of prograde bed slope. Additionally, through analytic expressions for marine-terminating glacier sensitivity to forcing, we show that stronger nonlinearity in forcing processes make glaciers more sensitive to external forcing. As we argue in section 4.2, the timing of forcing onset may also have a significant influence on the current magnitude and rate of glacier response, even for glaciers that are otherwise identical.

The observed retreat and thinning of marine-terminating glaciers in recent decades is striking, but should be interpreted within the context of expected glacier variability forced by stationary stochastic variability in ocean and atmospheric forcing. A few longer records of marine-terminating glacier variability (up to 150 years) have been constructed from airborne and field observations [e.g., Yde and Knudsen, 2007; Csatho *et al.*, 2008; Weidick *et al.*, 2012; Bjørk *et al.*, 2012; Leclercq *et al.*, 2012; Lea *et al.*, 2014; Leclercq *et al.*, 2014]. Though such records are still not long enough to capture the slow time scale of marine-terminating glacier variability ($T_S > 1000$ years), detectable changes in atmospheric and ocean warming and the associated terminus retreat only began in the last few decades at most calving glaciers [Bjørk *et al.*, 2012; Leclercq *et al.*, 2014]. Even if natural variability of these glaciers is large, it is only expressed on long time scales. Forced change on shorter time scales may exhibit a faster rate of change than what can be reliably attributed to natural variability. We intend to explore such questions of detection and attribution in future work.

870 The lack of observed thinning and retreat at some glaciers [e.g. Petermann Glacier
871 and ice streams in the western Ross Sea region, see *Hogg et al.*, 2016; *Fountain et al.*,
872 2017] does not necessarily preclude future thinning and retreat occurring on the slow time
873 scale of hundreds to thousands of years. Indeed, as we have shown (section 4.2), recent
874 changes at these stable marine-terminating glaciers are just a small fraction of the total
875 committed retreat expected in the future in response to climate change that has already oc-
876 curred. If the trend in climate forcing continues over the next century, there will be many
877 marine-terminating glaciers where the speed of glacier change will accelerate significantly.
878 Even past changes in climate that do not continue into the future cause a “commitment”
879 to future changes in marine-terminating glaciers that persists for hundreds to thousands of
880 years.

881 **6.2 Model flexibility and simplicity**

882 The flexibility of the two-stage model has allowed us to analyze the physical pro-
883 cesses controlling the response of marine-terminating glaciers to forcing. This flexibility
884 is premised on the assumptions that mass enters the glacier through a spatially-averaged
885 surface mass balance and leaves via flux through the grounding line, where that flux is a
886 function of the local ice thickness at flotation. Most of our analysis does not require any
887 further assumptions regarding the physical processes in the grounding zone. Thus, the
888 two-stage model and the associated linear analysis can accommodate a variety of differ-
889 ent types of marine-terminating glaciers, including those with strong lateral shear stresses
890 [*Hindmarsh*, 2012], Weertman basal sliding [*Schoof*, 2007a], Coulomb plastic failure near
891 the grounding line [*Tsai et al.*, 2015] or strong buttressing by ice shelves [*Haseloff and*
892 *Sergienko*, 2018].

893 There are some drawbacks to the simplicity of the two-stage model. Our model for-
894 mulation implicitly assumes that the glacier is marine-terminating and always remains
895 marine-terminating. Also, as we have shown in section 2.2, the two-stage model emulates
896 the transient behavior of a flowline model at time scales longer than a few decades. How-
897 ever, the flowline model is itself a simplification of real marine-terminating glacier pro-
898 cesses, for which there are very few observations. It is difficult to compare the two-stage
899 model directly to observations, since we have shown that the largest changes in stable
900 marine-terminating glaciers occur on time scales that are much longer than the length of
901 available observational time series. We have also shown that the two-stage model may not

902 be entirely reliable for reproducing glacier fluctuations on time scales shorter than a few
 903 decades, though the magnitude of glacier response at these short time scales is small (and
 904 it is unclear how well fast glacier fluctuations are simulated in the flowline model). Fur-
 905 thermore, the flux formulation we use [from *Haseloff and Sergienko, 2018*] integrates the
 906 effects of buttressing over the entire ice shelf by assuming that it is at a steady-state, and
 907 so neglects time-dependent adjustment processes occurring within the ice shelf. A fully-
 908 coupled model of an ice sheet and ice shelf would likely have an additional time scale
 909 associated with ice shelf adjustment processes.

910 One possible future extension of the two-stage model would be to formulate the lin-
 911 ear response problem outlined in section 3 for the spatially-extended shelfy-stream equa-
 912 tions (what is solved by the flowline model described in section 2.2). One could then find
 913 the spatially-dependent glacier response to external forcing with a generic spatial structure
 914 (rather than the spatially-uniform forcing used in the two-stage model), which may include
 915 very rapid glacier responses (i.e. shorter than the fast time scale T_F) to spatially-localized
 916 forcing.

917 There are also clear limits to the use of a linear theory to capture the complexity
 918 of bed topography. In our linearized analysis, we assume that the width-averaged depth
 919 and slope of the bed at the grounding line remains relatively unchanged under changes
 920 in glacier state. This may be most appropriate for beds with relatively weak topographic
 921 variation such as those in West Antarctica, and less appropriate for beds with strong to-
 922 pographic variation, such as those in parts of Greenland. We can, however, still use the
 923 two-stage model to calculate the grounding-line migration over these bumpy beds. We
 924 may also use an “average” depth and bed slope over the region of bed that we expect the
 925 grounding line to migrate, which will improve the linear prediction of grounding-line mi-
 926 gration over bumpy beds on long time scales.

927 We have also left out other processes, such as isostatic bedrock adjustment, that may
 928 be important on the long time scales over which marine-terminating glaciers respond to
 929 forcing. Feedbacks between surface mass balance and geometry, such as the height-mass
 930 balance feedback, may also play a role. To incorporate such effects [as does *Harrison*
 931 *et al., 2003*], we might replace the surface mass balance term (P) in equation 8, with a
 932 term that depends on H and L . In this study, we consider the limit where the sensitivity
 933 of ice fluxes to changes in ice sheet geometry (e.g., $\frac{\partial Q_g}{\partial L}$ and $\frac{\partial Q}{\partial H}$) is much more impor-

934 tant to glacier evolution than the sensitivity of surface mass balance to changes in geom-
935 etry ($\frac{\partial P}{\partial H}$). However, we do not rule out the possibility that when the vertical gradient in
936 surface mass balance gradient is large (due to orographic or other local climate effects),
937 this effect may be important. The virtue of the two-stage model presented here is that the
938 essence of the dynamical system can be identified and explored. These essential dynam-
939 ics will also operate in more complicated numerical models, in addition to the real glacier
940 system.

941 **7 Conclusions**

942 We have shown that a simple two-stage model can emulate the transient response of
943 a marine-terminating glacier simulated in a spatially-extended model, particularly at time
944 scales longer than a few decades. In both the two-stage and spatially-extended models, the
945 response of a marine-terminating glacier to forcing is dominated by two time scales. The
946 fast time scale is controlled by the rate of advective adjustment to changes in ice thick-
947 ness, and is typically decades to centuries. The slow time scale is controlled by the rate
948 at which ice thickness perturbations are dissipated by differences in advective and exten-
949 sional adjustment in the grounding zone, and is typically millennia. The slow time scale
950 becomes unstable on shallow prograde slopes and the fast time scale becomes unstable on
951 steep retrograde slopes, producing two distinct forms of the marine ice sheet instability.

952 We have derived simple expressions for the magnitude of glacier response to differ-
953 ent types of forcing that can be calculated without resorting to use of a complex numer-
954 ical glacier model. The strength of the response depends on the glacier state, the time-
955 averaged forcing, and the strength of nonlinearity in ice dynamical processes. A stable
956 marine-terminating glacier responds slowly to the onset of a trend in forcing and will only
957 begin to approach the long-term expected rate of change on the slow time scale of cen-
958 turies to millennia. We expect that the current level of stable marine-terminating glacier
959 retreat is a small fraction of the “committed” retreat that can be expected as the rate of
960 glacier change accelerates in coming centuries [as has been shown for many mountain
961 glaciers, e.g. *Rupper et al.*, 2012]. Even stable glaciers which have not yet undergone
962 detectable change may undergo such change in the future as the glaciers catch up to the
963 forcing. The slow glacier response to stochastic external forcing suggests that the rate,
964 rather than the absolute level, of glacier change caused by trends in forcing are potentially
965 more easily discernible from background noise. Finally, we have shown that the equilib-

966 rium state of a marine-terminating glacier depends on the magnitude of noise in nonlinear
967 forcing processes, such as ice-shelf length variations that occur through calving.

968 One important conclusion of this study is that the slow time scale of marine-terminating
969 glacier change ensures that uncertainties in climate forcing (either in the past or future) in-
970 fluence glacier change for hundreds to thousands of years. To account for the uncertainties
971 associated with future climate forcing in simulating ice-sheet change will require large en-
972 sembles of stochastic ice-sheet model simulations that result in probabilistic forecasts of
973 future sea-level rise. Though studies such as the SeaRISE project consider uncertainties
974 in ice-sheet physics through small multi-model ensembles with common forcing [*Bind-*
975 *schadler et al.*, 2013], they do not capture the uncertainty in future projections associated
976 with the forcing itself [e.g., *Tsai et al.*, 2017]. As we have shown, considering noise is not
977 just important for constraining the background envelope of variability, but also for accu-
978 rately simulating the time-averaged glacier state. For one, if the magnitude of noise in cer-
979 tain ice sheet processes changes over time (e.g., as the style of iceberg calving from an ice
980 shelf changes), this may drive glacier retreat that would not be predicted in the absence
981 of noise. Also, model spin-up and calibration performed without natural sources of noisy
982 forcing (or forcing with a truncated spectrum of variability due to asynchronous model
983 coupling) may lead to unrealistic glacier states. As a new generation of fully-coupled cli-
984 mate and ice-sheet models are used to produce projections of future ice-sheet change, it is
985 important to consider the ice-sheet response to high-frequency climate variability through
986 nearly synchronous coupling. To exclude the noise of climate when predicting future ice-
987 sheet change misses an important piece of the glaciological puzzle.

988 **Acknowledgments**

989 Source code and documentation of the two-stage and flowline models used in this study
990 are freely available as public repositories on GitHub: <https://github.com/aarobel/>. Thanks
991 to Olga Sergienko, Martin Truffer, Jeremy Bassis and Elisa Mantelli for helpful comments
992 on the manuscript. This work was initially conceived through a series of conversations at
993 the 2014 Advanced Climate Dynamics Course, which is coordinated by the Norwegian
994 Research School in Climate Dynamics (ResClim). Thanks to Nicholas Beaird, Bradley
995 Markle and Andreas Vieli for taking part in those initial conversations. The authors also
996 thank Christian Schoof, Victor Tsai, Georgy Manucharyan, John Christian, Denis Felikson
997 and Ian Joughin for subsequent conversations and suggestions. AAR was supported by the

998 NOAA Climate and Global Change Postdoctoral Fellowship during part of this project.
999 GHR acknowledges support from NSF PLR-1643299. MH was supported by the Princeton
1000 AOS Postdoctoral and Visiting Scientist Program.

1001 **References**

- 1002 Amundson, J. M. (2016), A mass-flux perspective of the tidewater glacier cycle, *Journal*
1003 *of Glaciology*, *62*(231), 82–93.
- 1004 Bassis, J. N. (2011), The statistical physics of iceberg calving and the emergence of uni-
1005 versal calving laws, *Journal of Glaciology*, *57*(201), 3–16.
- 1006 Bindshadler, R. A., S. Nowicki, A. Abe-Ouchi, A. Aschwanden, H. Choi, J. Fastook,
1007 G. Granzow, R. Greve, G. Gutowski, U. Herzfeld, et al. (2013), Ice-sheet model sen-
1008 sitivities to environmental forcing and their use in projecting future sea level (the
1009 SeaRISE project), *Journal of Glaciology*, *59*(214), 195–224.
- 1010 Bjørk, A. A., K. H. Kjær, N. J. Korsgaard, S. A. Khan, K. K. Kjeldsen, C. S. Andresen,
1011 N. K. Larsen, and S. Funder (2012), An aerial view of 80 years of climate-related
1012 glacier fluctuations in southeast Greenland, *Nature Geoscience*, *5*(6), 427–432.
- 1013 Box, G., G. Jenkins, G. Reinsel, and G. Ljung (2015), *Time Series Analysis: Forecasting*
1014 *and Control*, Wiley Series in Probability and Statistics, Wiley.
- 1015 Brinkerhoff, D., M. Truffer, and A. Aschwanden (2017), Sediment transport drives tidewa-
1016 ter glacier periodicity, *Nature Communications*, *8*(1), 90.
- 1017 Brondex, J., O. Gagliardini, F. Gillet-Chaulet, and G. Durand (2017), Sensitivity of
1018 grounding line dynamics to the choice of the friction law, *Journal of Glaciology*,
1019 *63*(241), 854–866.
- 1020 Csatho, B., T. Schenk, C. J. Van Der Veen, and W. B. Krabill (2008), Intermittent thinning
1021 of Jakobshavn Isbrae, West Greenland, since the Little Ice Age, *Journal of Glaciology*,
1022 *54*(184), 131–144.
- 1023 Csatho, B. M., A. F. Schenk, C. J. van der Veen, G. Babonis, K. Duncan, S. Rezvanbe-
1024 hbahani, M. R. Van Den Broeke, S. B. Simonsen, S. Nagarajan, and J. H. van Angelen
1025 (2014), Laser altimetry reveals complex pattern of greenland ice sheet dynamics, *Pro-*
1026 *ceedings of the National Academy of Sciences*, *111*(52), 18,478–18,483.
- 1027 Cuffey, K., and W. Paterson (2010), *The Physics of Glaciers*, 3rd ed., 480 pp., Pergamon.
- 1028 Drouet, A.-S., D. Docquier, G. Durand, R. Hindmarsh, F. Pattyn, O. Gagliardini, and
1029 T. Zwinger (2013), Grounding line transient response in marine ice sheet models, *The*

- 1030 *Cryosphere*, 7(2), 395–406.
- 1031 Favier, L., G. Durand, S. Cornford, G. Gudmundsson, O. Gagliardini, F. Gillet-Chaulet,
1032 T. Zwinger, A. Payne, and A. Le Brocq (2014), Retreat of Pine Island Glacier con-
1033 trolled by marine ice-sheet instability, *Nature Climate Change*.
- 1034 Felikson, D., T. C. Bartholomaus, G. A. Catania, N. J. Korsgaard, K. H. Kjær,
1035 M. Morlighem, B. Noël, M. van den Broeke, L. A. Stearns, E. L. Shroyer, D. A. Suther-
1036 land, and J. D. Nash (2017), Inland thinning on the Greenland ice sheet controlled by
1037 outlet glacier geometry, *Nature Geoscience*, 10, 366–369.
- 1038 Fettweis, X. (2007), Reconstruction of the 1979–2006 Greenland ice sheet surface mass
1039 balance using the regional climate model MAR, *The Cryosphere*, 1(1), 21–40.
- 1040 Fountain, A. D., B. Glenn, and T. A. Scambos (2017), The changing extent of the glaciers
1041 along the western Ross Sea, Antarctica, *Geology*, doi:10.1130/G39240.1.
- 1042 Fyke, J. G., M. Vizcaíno, and W. H. Lipscomb (2014), The pattern of anthropogenic sig-
1043 nal emergence in Greenland Ice Sheet surface mass balance, *Geophysical Research Let-
1044 ters*, 41(16), 6002–6008.
- 1045 Gomez, N., J. X. Mitrovica, P. Huybers, and P. U. Clark (2010), Sea level as a stabilizing
1046 factor for marine-ice-sheet grounding lines, *Nature Geoscience*, 3(12), 850–853.
- 1047 Gudmundsson, G., J. Krug, G. Durand, L. Favier, and O. Gagliardini (2012), The stability
1048 of grounding lines on retrograde slopes, *The Cryosphere*, 6(4), 2597–2619.
- 1049 Harrison, W. D., C. F. Raymond, K. A. Echelmeyer, and R. M. Krimmel (2003), A macro-
1050 scopic approach to glacier dynamics, *Journal of Glaciology*, 49(164), 13–21.
- 1051 Haseloff, M., and O. V. Sergienko (2018), The effect of buttressing on grounding line dy-
1052 namics, *Journal of Glaciology*, 64(245), 417–431, doi:10.1017/jog.2018.30.
- 1053 Hindmarsh, R., and E. Le Meur (2001), Dynamical processes involved in the retreat of
1054 marine ice sheets, *Journal of Glaciology*, 47(157), 271–282.
- 1055 Hindmarsh, R. C. (2012), An observationally validated theory of viscous flow dynamics at
1056 the ice-shelf calving front, *Journal of Glaciology*, 58(208), 375–387.
- 1057 Hogg, A. E., A. Shepherd, N. Gourmelen, and M. Engdahl (2016), Grounding line mi-
1058 gration from 1992 to 2011 on Petermann Glacier, North-West Greenland, *Journal of
1059 Glaciology*, 62(236), 1104–1114.
- 1060 IPCC (2013), *Climate Change 2013: The Physical Science Basis. Contribution of Work-
1061 ing Group I to the Fifth Assessment Report of the Intergovernmental Panel on Climate
1062 Change*, 1535 pp., Cambridge University Press, Cambridge, United Kingdom and New

- 1063 York, NY, USA, doi:10.1017/CBO9781107415324.
- 1064 Jamieson, S., A. Vieli, S. Livingstone, C. Cofaigh, C. Stokes, C. Hillenbrand, and
1065 J. Dowdeswell (2012), Ice-stream stability on a reverse bed slope, *Nature Geoscience*,
1066 5(11), 799–802.
- 1067 Jóhannesson, T., C. Raymond, and E. Waddington (1989), Time-scale for adjustment of
1068 glaciers to changes in mass balance, *Journal of Glaciology*, 35(121), 355–369.
- 1069 Joughin, I., I. M. Howat, M. Fahnestock, B. Smith, W. Krabill, R. B. Alley, H. Stern,
1070 and M. Truffer (2008), Continued evolution of Jakobshavn Isbræ following its rapid
1071 speedup, *Journal of Geophysical Research: Earth Surface*, 113(F4).
- 1072 Joughin, I., B. E. Smith, I. M. Howat, T. Scambos, and T. Moon (2010), Greenland flow
1073 variability from ice-sheet-wide velocity mapping, *Journal of Glaciology*, 56(197), 415–
1074 430.
- 1075 Joughin, I., R. B. Alley, and D. M. Holland (2012), Ice-sheet response to oceanic forcing,
1076 *Science*, 338(6111), 1172–1176.
- 1077 Larsen, S. H., S. A. Khan, A. P. Ahlstrøm, C. S. Hvidberg, M. J. Willis, and S. B. Ander-
1078 sen (2016), Increased mass loss and asynchronous behavior of marine-terminating outlet
1079 glaciers at Upernavik Isstrøm, NW Greenland, *Journal of Geophysical Research: Earth*
1080 *Surface*, 121(2), 241–256.
- 1081 Lea, J., D. Mair, F. Nick, B. Rea, D. Van As, M. Morlighem, P. Nienow, and A. Wei-
1082 dick (2014), Fluctuations of a Greenlandic tidewater glacier driven by changes in atmo-
1083 spheric forcing: observations and modelling of Kangiata Nunaata Sermia, 1859–present,
1084 *The Cryosphere Discussions*.
- 1085 Leclercq, P., A. Weidick, F. Paul, T. Bolch, M. Citterio, and J. Oerlemans (2012), Brief
1086 communication: Historical glacier length changes in West Greenland, *The Cryosphere*,
1087 6, 1339–1343.
- 1088 Leclercq, P. W., J. Oerlemans, H. J. Basagic, I. Bushueva, A. Cook, and R. Le Bris
1089 (2014), A data set of worldwide glacier length fluctuations, *The Cryosphere*, 8(2), 659–
1090 672.
- 1091 Lenton, T. M. (2011), Early warning of climate tipping points, *Nature Climate Change*,
1092 1(4), 201–209.
- 1093 Lingle, C. S. (1984), A numerical model of interactions between a polar ice stream and
1094 the ocean: Application to ice stream E, West Antarctica, *Journal of Geophysical Re-*
1095 *search: Oceans*, 89(C3), 3523–3549.

- 1096 Lüthi, M. P. (2009), Transient response of idealized glaciers to climate variations, *Journal*
1097 *of Glaciology*, 55(193), 918–930.
- 1098 Mantelli, E., M. B. Bertagni, and L. Ridolfi (2016), Stochastic ice stream dynamics, *Pro-*
1099 *ceedings of the National Academy of Sciences*, 113(32), E4594–E4600.
- 1100 Marzeion, B., J. G. Cogley, K. Richter, and D. Parkes (2014), Attribution of global glacier
1101 mass loss to anthropogenic and natural causes, *Science*, 345(6199), 919–921.
- 1102 Mernild, S. H., T. L. Mote, and G. E. Liston (2011), Greenland ice sheet surface melt ex-
1103 tent and trends: 1960–2010, *Journal of Glaciology*, 57(204), 621–628.
- 1104 Mikkelsen, T. B., A. Grinsted, and P. Ditlevsen (2017), Influence of temperature fluctu-
1105 ations on equilibrium ice sheet volume, *The Cryosphere Discussions*, 2017, 1–16, doi:
1106 10.5194/tc-2017-47.
- 1107 Moon, T., I. Joughin, and B. Smith (2015), Seasonal to multiyear variability of glacier
1108 surface velocity, terminus position, and sea ice/ice mélange in northwest Greenland,
1109 *Journal of Geophysical Research: Earth Surface*, 120(5), 818–833.
- 1110 Motyka, R. J., R. Cassotto, M. Truffer, K. K. Kjeldsen, D. Van As, N. J. Korsgaard,
1111 M. Fahnestock, I. Howat, P. L. Langen, J. Mortensen, et al. (2017), Asynchronous be-
1112 havior of outlet glaciers feeding Godthåbsfjord (Nuup Kangerlua) and the triggering of
1113 Narsap Sermia’s retreat in SW Greenland, *Journal of Glaciology*, 63(238), 288–308.
- 1114 Mulder, T. E., S. Baars, F. W. Wubs, and H. A. Dijkstra (2018), Stochastic marine ice
1115 sheet variability, *Journal of Fluid Mechanics*, 843, 748?777, doi:10.1017/jfm.2018.148.
- 1116 Nick, F., C. J. Van der Veen, A. Vieli, and D. Benn (2010), A physically based calving
1117 model applied to marine outlet glaciers and implications for the glacier dynamics, *Jour-*
1118 *nal of Glaciology*, 56(199), 781–794.
- 1119 Nicolis, C., and G. Nicolis (1981), Stochastic aspects of climatic transitions—additive fluc-
1120 tuations, *Tellus*, 33(3), 225–234.
- 1121 Nye, J. (1960), The response of glaciers and ice-sheets to seasonal and climatic changes,
1122 *Proceedings of the Royal Society of London A: Mathematical, Physical and Engineering*
1123 *Sciences*, 256(1287), 559–584.
- 1124 Nye, J. (1963a), On the theory of the advance and retreat of glaciers, *Geophysical Journal*
1125 *International*, 7(4), 431–456.
- 1126 Nye, J. (1963b), The response of a glacier to changes in the rate of nourishment and
1127 wastage, *Proceedings of the Royal Society of London A: Mathematical, Physical and Engi-*
1128 *neering Sciences*, 275(1360), 87–112.

- 1129 Nye, J. F. (1965), The frequency response of glaciers, *Journal of Glaciology*, 5(41), 567–
1130 587.
- 1131 Oerlemans, J. (2000), Holocene glacier fluctuations: is the current rate of retreat excep-
1132 tional?, *Annals of Glaciology*, 31(1), 39–44.
- 1133 Park, J., N. Gourmelen, A. Shepherd, S. Kim, D. Vaughan, and D. Wingham (2013), Sus-
1134 tained retreat of the Pine Island Glacier, *Geophysical Research Letters*, 40(10), 2137–
1135 2142.
- 1136 Pattyn, F., C. Schoof, L. Perichon, R. Hindmarsh, E. Bueller, B. d. Fleurian, G. Durand,
1137 O. Gagliardini, R. Gladstone, D. Goldberg, et al. (2012), Results of the marine ice sheet
1138 model intercomparison project, MISMIP, *The Cryosphere*, 6(3), 573–588.
- 1139 Pegler, S. S. (2016), The dynamics of confined extensional flows, *Journal of Fluid Me-*
1140 *chanics*, 804, 24–57.
- 1141 Pelto, M. S., and C. R. Warren (1991), Relationship between tidewater glacier calving ve-
1142 locity and water depth at the calving front, *Annals of Glaciology*, 15, 115–118.
- 1143 Penland, C. (2003), A stochastic approach to nonlinear dynamics: A review, *Bulletin of the*
1144 *American Meteorological Society*, 84(7), 925–925.
- 1145 Post, A., and R. J. Motyka (1995), Taku and le conte glaciers, alaska: Calving-speed con-
1146 trol of late-holocene asynchronous advances and retreats, *Physical Geography*, 16(1),
1147 59–82.
- 1148 Pritchard, H. D., R. J. Arthern, D. G. Vaughan, and L. A. Edwards (2009), Extensive
1149 dynamic thinning on the margins of the Greenland and Antarctic ice sheets, *Nature*,
1150 461(7266), 971–975.
- 1151 Rignot, E., M. Koppes, and I. Velicogna (2010), Rapid submarine melting of the calving
1152 faces of West Greenland glaciers, *Nature Geoscience*, 3(3), 187–191.
- 1153 Robel, A., C. Schoof, and E. Tziperman (2014), Rapid grounding line migration induced
1154 by internal ice stream variability, *J. Geophys. Res.*, 119, 2430–2447.
- 1155 Roe, G. H., and M. B. Baker (2014), Glacier response to climate perturbations: an accu-
1156 rate linear geometric model, *Journal of Glaciology*, 60(222), 670–684.
- 1157 Roe, G. H., and M. B. Baker (2016), The response of glaciers to climatic persistence,
1158 *Journal of Glaciology*, 62(233), 440–450.
- 1159 Roe, G. H., and M. A. O’Neal (2009), The response of glaciers to intrinsic climate vari-
1160 ability: observations and models of late-Holocene variations in the Pacific Northwest,
1161 *Journal of Glaciology*, 55(193), 839–854.

- 1162 Roe, G. H., M. B. Baker, and F. Herla (2017), Centennial glacier retreat as categorical
1163 evidence of regional climate change, *Nature Geoscience*, *10*(2), 95–99.
- 1164 Rupper, S., J. M. Schaefer, L. K. Burgener, L. S. Koenig, K. Tsering, and E. R. Cook
1165 (2012), Sensitivity and response of Bhutanese glaciers to atmospheric warming, *Geo-*
1166 *physical Research Letters*, *39*(19).
- 1167 Scheuchl, B., J. Mouginot, E. Rignot, M. Morlighem, and A. Khazendar (2016), Ground-
1168 ing line retreat of Pope, Smith, and Kohler Glaciers, West Antarctica, measured with
1169 Sentinel-1a radar interferometry data, *Geophysical Research Letters*, *43*(16), 8572–8579.
- 1170 Schodlok, M. P., D. Menemenlis, E. Rignot, and M. Studinger (2012), Sensitivity of the
1171 ice-shelf/ocean system to the sub-ice-shelf cavity shape measured by NASA IceBridge
1172 in Pine Island Glacier, West Antarctica, *Annals of Glaciology*, *53*(60), 156–162.
- 1173 Schoof, C. (2006), A variational approach to ice stream flow, *J. Fluid Mech.*, *556*, 227–
1174 251, doi:10.1017/S0022112006009591.
- 1175 Schoof, C. (2007a), Marine ice-sheet dynamics. Part 1. The case of rapid sliding, *J. Fluid*
1176 *Mech.*, *573*, 27–55, doi:10.1017/S0022112006003570.
- 1177 Schoof, C. (2007b), Ice sheet grounding line dynamics: Steady states, stability,
1178 and hysteresis, *Journal of Geophysical Research - Earth Surface*, *112*(F3), doi:
1179 10.1029/2006JF000664.
- 1180 Schoof, C. (2012), Marine ice sheet stability, *Journal of Fluid Mechanics*, *698*, 62–72.
- 1181 Schoof, C., A. D. Davis, and T. V. Popa (2017), Boundary layer models for calving marine
1182 outlet glaciers, *The Cryosphere Discussions*, *2017*, 1–30, doi:10.5194/tc-2017-42.
- 1183 Sciascia, R., F. Straneo, C. Cenedese, and P. Heimbach (2013), Seasonal variability of
1184 submarine melt rate and circulation in an East Greenland fjord, *Journal of Geophysical*
1185 *Research: Oceans*, *118*(5), 2492–2506.
- 1186 Seroussi, H., Y. Nakayama, E. Larour, D. Menemenlis, M. Morlighem, E. Rignot, and
1187 A. Khazendar (2017), Continued retreat of Thwaites Glacier, West Antarctica, controlled
1188 by bed topography and ocean circulation, *Geophysical Research Letters*.
- 1189 Suzuki, M. (1977), Scaling theory of transient phenomena near the instability point, *Jour-*
1190 *nal of Statistical Physics*, *16*(1), 11–32.
- 1191 Tsai, C.-Y., C. E. Forest, and D. Pollard (2017), Assessing the contribution of internal cli-
1192 mate variability to anthropogenic changes in ice sheet volume, *Geophysical Research*
1193 *Letters*.

- 1194 Tsai, V. C., A. L. Stewart, and A. F. Thompson (2015), Marine ice-sheet profiles and sta-
1195 bility under coulomb basal conditions, *Journal of Glaciology*, *61*(226), 205–215.
- 1196 van der Veen, C. (2001), Greenland ice sheet response to external forcing, *Journal of Geo-*
1197 *physical Research: Atmospheres*, *106*(D24), 34,047–34,058.
- 1198 Velicogna, I. (2009), Increasing rates of ice mass loss from the Greenland and Antarctic
1199 ice sheets revealed by GRACE, *Geophysical Research Letters*, *36*(19).
- 1200 Weertman, J. (1957), On the sliding of glaciers, *Journal of Glaciology*, *3*(21), 33–38.
- 1201 Weertman, J. (1974), Stability of the junction of an ice sheet and an ice shelf, *Journal of*
1202 *Glaciology*, *13*, 3–11.
- 1203 Weidick, A., O. Bennike, M. Citterio, and N. Nørgaard-Pedersen (2012), Neoglacial and
1204 historical glacier changes around Kangarsuneq Fjord in southern West Greenland, *Geo-*
1205 *logical Survey of Denmark and Greenland Bulletin*, *27*, 68.
- 1206 Wouters, B., A. Martin-Español, V. Helm, T. Flament, J. van Wessem, S. Ligtenberg,
1207 M. van den Broeke, and J. Bamber (2015), Dynamic thinning of glaciers on the South-
1208 ern Antarctic Peninsula, *Science*, *348*(6237), 899–903.
- 1209 Yde, J. C., and N. T. Knudsen (2007), 20th-century glacier fluctuations on Disko Island
1210 (Qeqertarsuaq), Greenland, *Annals of Glaciology*, *46*(1), 209–214.